



Diese Diplomarbeit wurde begutachtet von:

Prof. Dr. K. Held

D I P L O M A R B E I T

Continuous-Time Quantum Monte Carlo

Implementation of a Measurement Routine for a Two-Particle
Correlation Function in a Hybridization Algorithm

Ausgeführt zum Zwecke der Erlangung des akademischen Grades eines
Diplom Ingenieurs unter der Leitung von

Prof. Dr. Karsten Held

&

Dr. Giorgio Sangiovanni (1. betreuender Assistent)

&

Dipl.-Ing. Nico Parragh (2. betreuender Assistent)

E138 - Institut für Festkörperphysik

Eingereicht an der Technischen Universität Wien
Fakultät für Physik

von

Christian Ecker

Matrikelnummer: 0526161
Blütengasse 9/2/22, 1030 Wien

Wien, am 08.05.2013

Christian Ecker

Abstract

The primary objective of this work was the implementation of a measurement routine for the two-particle Green's function in a Continuous-Time Quantum Monte Carlo code. We start with a brief discussion of the Hubbard model and the Anderson impurity model in their multi-band realizations. After that a short introduction to Dynamical Mean-Field Theory is given. A general discussion of the Continuous-Time Quantum Monte Carlo method is followed by a detailed exposition of the hybridization algorithm. The major advantage of the hybridization algorithm, compared to the well established Hirsch-Fye method is, that complex multi-band interactions with off-diagonal elements in Fock space like the Coulomb interaction can be implemented straight forwardly. Furthermore one is not restricted to a finite number of bath sites as in the Exact-Diagonalization method. Based on the action formulation of the Anderson impurity model we give a formal derivation of the Continuous-Time Quantum Monte Carlo measurement formulas for the single-particle and two-particle Green's function. The derived formulas for are used to implement and test a measurement routine for the two-particle Green's function in an existing code. We compare numerical results from our routine to those from a Hirsch-Fye and an Exact-Diagonalization code. As a first application we calculate the local spin susceptibility at the metal-insulator Mott-transition of the half-filled single-band Hubbard model. An extensive treatment of the Coulomb interaction Hamiltonian can be found in the appendix.

Zusammenfassung

Das primäre Ziel dieser Arbeit bestand in der Implementierung einer Messroutine für die Zweiteilchen-Greensfunktion in einem Continuous-Time Quanten Monte Carlo Code. Ausgehend von einer kurzen Erläuterung des Hubbard-Modells und des Anderson-Störstellen-Modells mit besonderem Augenmerk auf deren Mehrband-Ausführungen folgt eine Einführung in die Dynamische Molekularfeldtheorie. Nach einer allgemeinen Erörterung der Continuous-Time Quanten Monte Carlo Methode findet sich eine detaillierte Diskussion des Hybridisierungsalgorithmus. Als wesentlicher Vorteil des Hybridisierungsalgorithmus im Vergleich zum Hirsch-Fye-Algorithmus zeigt sich, dass Mehrbandwechselwirkungen die nicht vom Dichte-Dichte Typ sind (z.B. Coulomb Wechselwirkung) relativ einfach implementiert werden können. Ausgehend von der Wirkung des Anderson-Störstellen-Modells präsentieren wir eine formale Herleitung der Messformeln für die Ein- und Zweiteilchen Greensfunktion. Basierend auf diesen Formeln wurde eine Routine zum Messen der Zweiteilchen-Greensfunktion implementiert und getestet. Anschließend wurden die numerischen Ergebnisse von dieser Routine mit den Ergebnissen des Hirsch-Fye Algorithmus und der Methode der Exakten Diagonalisierung verglichen. Als erste Anwendung unserer Routine wird die Spinsuszeptibilität in der Nähe des Metall-Isolator-Mott-Überganges des halbgefüllten Hubbard Modells berechnet. Im Anhang findet sich eine ausführliche Herleitung der Matrix-Elemente des Coulomb Hamiltonoperators.

Acknowledgments

First of all I would like to thank Prof. Karsten Held for giving me the opportunity of writing this thesis in his working group. I am especially grateful for pointing out some weak-points in my derivation of the measurement formulas and for the final remarks on my manuscript. Further, I thank Giorgio Sangiovanni for leading me to the references for a first reading on the topic of this thesis. His help with interpreting the first CTQMC results and pointing to possible sources of error were invaluable in debugging the code. I also would like to thank Nico Paragh for setting up the CTQMC code including the measurement routine for the single-particle Green's function. This thesis actually represents only a small extension of Nico's work and would have definitely not been possible without his permanent support. Angelo Valli provided the results from the Hirsch-Fye solver and the routine for doing the Fourier transformation. I am very grateful for his support and the inspiring discussions with him. I thank Georg Rohringer for providing the results from the Exact-Diagonalization solver. These results have been of great value in checking whether the CTQMC code works correctly. Finally I would like to thank my family, Daniela and Mia-Josephine, for their understanding, patience, and support.

Contents

| | | |
|----------|--|-----------|
| 1 | Introduction | 1 |
| 2 | Microscopic Description of Strongly Correlated Electron Systems | 3 |
| 2.1 | Quantum Impurity Models | 6 |
| 2.2 | Finite Temperature Green's Functions | 8 |
| 3 | Dynamical Mean-Field Theory | 17 |
| 3.1 | The Limit of Infinite Dimensions | 18 |
| 3.2 | Self-Consistent Mapping onto Impurity Model | 22 |
| 4 | Continuous-Time Quantum Monte Carlo | 27 |
| 4.1 | The Hybridization Expansion | 28 |
| 4.2 | Monte Carlo Sampling of the Partition Function | 32 |
| 4.3 | Measuring Correlation Functions | 36 |
| 5 | Numerical Simulations | 41 |
| 5.1 | Two-Particle Quantities in τ -space | 41 |
| 5.2 | Generalized Susceptibilities in Frequency-space | 44 |
| 5.3 | Performance Benchmark | 46 |
| 5.4 | First Application: Local Spin Susceptibility | 48 |
| 6 | Conclusion and Prospect | 52 |
| | Bibliography | 55 |
| A | The Local Hamiltonian for Spherical Symmetric Coulomb Interaction | 58 |
| A.1 | The Wigner 3-j Symbol | 59 |
| A.2 | Gaunt Coefficients | 60 |
| A.3 | The Matrix Elements of Coulomb Interaction | 60 |

| | | |
|----------|---|-----------|
| B | Derivation of Bare Green's Functions using the Equation of Motion Method | 64 |
| B.1 | Bare Green's Function of the Hubbard Model | 64 |
| B.2 | Bare Green's Function of the Anderson Impurity Hamiltonian | 68 |
| C | The Partition Function Expansion | 70 |
| D | The Derivative of a Determinant | 73 |
| E | Hirsch-Fye Method | 74 |

Chapter 1

Introduction

The goal of computational material science (CMS) is the numerical simulation of physical phenomena in the field of condensed matter physics. It is a remarkable fact, that for a wide variety of materials electronic correlation effects due to the Coulomb repulsion play an insignificant role. These materials can be described in the framework of density functional theory (DFT). DFT, however, fails when the material behavior is governed by strong electronic correlation effects. Narrow bands and highly located overlapping orbitals are typical characteristics of such systems. In this case the mean-field description of electronic correlations in form of an electron gas is too crude and one has to take electron-electron interactions explicitly into account. Fermionic lattice models such as the Hubbard model provide an adequate way to describe these strongly correlated electron systems. The access to numerical solutions of such quantum mechanic lattice models is, however, restricted to a small number of lattice sites and bands due to the exponential growth of the corresponding Hilbert space. In dynamical mean-field theory (DMFT) a lattice model is mapped onto a numerically solvable impurity model and a self-consistency condition. While reaching self-consistency generally takes only a small number ($O[10^1]$) of iterations, efficiently solving multi-band impurity models is numerically challenging and still a task of active research. Recently developed Continuous-Time Quantum Monte Carlo (CTQMC) solvers, as the hybridization algorithm (CT-HYB), exhibit a number of advantages compared to previous Exact-Diagonalization (ED) and Hirsch-Fye (HF) solvers, which motivated this work.

This thesis is structured as follows. In the first part of Chapter 2 we introduce several impurity models with different local interaction types. In the framework of statistical quantum mechanics the solutions to such

models are expressed in terms of many-particle Green's functions. In the second part of Chapter 2 we derive some important analytical properties of single- and two-particle Green's functions.

In Chapter 3 we give an introduction to DMFT. We renormalize the lattice Hamiltonian in infinite dimensions and argue diagrammatically the locality of the corresponding self-energy in this limit. We derive the DMFT self-consistency scheme which is of central importance for numerical simulations.

Chapter 4 is about the Continuous-Time Quantum Monte Carlo method in the hybridization expansion. We derive in detail the hybridization expansion of the impurity model partition function. After that we describe how this infinite series is sampled in a Monte Carlo procedure. Finally we use functional methods to derive the Monte Carlo measurement formulas of the single- and two-particle Green's function.

The results from our numerical simulations are presented and discussed in Chapter 5. Here we compare the DMFT two-particle Green's functions and generalized susceptibilities calculated with the CTQMC method to those from the HF and ED solver. We benchmark the performance of our routine for several values of the interaction strength and temperature. As a first application we calculate the local spin susceptibility in the vicinity of the metal-insulator Mott-transition of the frustrated single-band Hubbard model.

In Chapter 6 a conclusion is drawn and prospective applications are suggested.

In the Appendix we collect several derivations concerning the full Coulomb Hamiltonian, the hybridization expansion and bare Green's functions of the Anderson impurity model (AIM) and the Hubbard model. A short description of the Hirsch-Fye method is also included in the Appendix.

Chapter 2

Microscopic Description of Strongly Correlated Electron Systems

A macroscopic crystal is a composition of a huge number ($O[10^{23}]$) of interacting microscopic constituents, namely electrons and ions, where the latter are arranged on a lattice with a spacing of typically few Å. This makes a quantum mechanical treatment necessary.

Ab Initio Hamiltonian. A formal description from first principles in terms of a many-body Hamiltonian is in general possible:

$$H = \underbrace{\sum_i \frac{\nabla_{\mathbf{R}_i}^2}{2M_i} + \frac{1}{2} \sum_{i \neq j} \frac{e^2 Z_i Z_j}{|\mathbf{R}_i - \mathbf{R}_j|}}_{H_n} + \underbrace{\sum_i \frac{\nabla_{\mathbf{r}_i}^2}{2m_e}}_T + \underbrace{\frac{1}{2} \sum_{i \neq j} \frac{e^2}{|\mathbf{r}_i - \mathbf{r}_j|}}_{V_{ee}} - \underbrace{\sum_{i,j} \frac{e^2 Z_j}{|\mathbf{r}_i - \mathbf{R}_j|}}_{V_{ion}}. \quad (2.1)$$

This *ab initio* Hamiltonian contains purely ionic contributions (H_n) where M_i denotes the mass and eZ_i the charge of the ion with position vector \mathbf{R}_i ; the purely electronic terms T and V_{ee} accounting for the kinetic and Coulomb energy of the electrons with position vector \mathbf{r}_i and charge e ; and finally the Coulomb term V_{ion} describing the interaction between the electrons and the ions. Due to the Coulomb interaction terms, a closed solution of the corresponding Schrödinger equation for a macroscopic system is not available. Next we discuss some approximations that make at least a numerical solution possible.

Born-Oppenheimer Approximation. Many properties of solids are primarily the result of the complicated interplay between the electrons only. In the Born-Oppenheimer approximation [1], dating back to 1927, the electrons are, due to their small mass, supposed to be in an instantaneous equilibrium with the much heavier slowly moving ions. This allows to employ a product ansatz for the total many-body wave function in terms of a purely ionic and a purely electronic wave function $\Phi(\vec{r}, \vec{R})$, where in the latter only a parametric dependence of the ionic degrees of freedom remains:

$$[T + V_{ee} + V_{ion}]\Phi(\vec{r}, \vec{R}) = E(\vec{R})\Phi(\vec{r}, \vec{R}). \quad (2.2)$$

Density Functional Theory. For a wide variety of materials density functional theory in its local density approximation (LDA) turned out to be an unexpectedly successful approach of solving Eq.(2.2). DFT is based on the theorems first published by Pierre Hohenberg and Walter Kohn [2] in 1964, who state that for a given external potential V_{ion} and fixed electron number $N = \int n(\mathbf{r})d\mathbf{r}$, the ground state energy E of a many-electron system is an unique functional of the electron density $n(\mathbf{r})$:

$$E[n] = E_{kin}[n] + E_{xc}[n] + E_H[n] + E_{ion}[n], \quad (2.3)$$

which attains its minimum relative to variations $\delta n(\vec{r})$ at the equilibrium density $n_0(\mathbf{r})$:

$$E[n_0] = \min \left\{ E[n] \mid N = \int n(\vec{r})d\vec{r} \right\}. \quad (2.4)$$

The Hartree term $E_H[n] = \frac{1}{2} \int d^3r d^3r' V_{ee}(\mathbf{r} - \mathbf{r}') n(\mathbf{r}) n(\mathbf{r}')$ and the ionic term $E_{ion}[n] = \int d^3r V_{ion}(\mathbf{r}) n(\mathbf{r})$ are easily expressible through the electron density. This is, however, not possible for the kinetic part which is therefore substituted by the kinetic energy $E_{kin}[n]$ of the non-interacting electron gas and the exchange-correlation functional $E_{xc}[n]$ accounting for the difference to the exact kinetic energy of the interacting electron system and for the missing exchange part in the Hartree term. Since all the material specific information is contained in V_{ion} , the functional $E_{xc}[n]$ is the same for each many-electron system. Unfortunately the exact form of $E_{xc}[n]$ is unknown. In LDA the unknown functional E_{xc} is approximated with the one of the homogeneous electron gas (Jellium model):

$$E_{xc}[n] \stackrel{LDA}{\approx} -\frac{3e^2}{4\pi} \int d^3r n(\vec{r}) \sqrt{3\pi^2 n(\vec{r})}. \quad (2.5)$$

In 1965 Walter Kohn and Lu Jeu Sham [3] state that the ground state electron density $n_0(\vec{r}) = \sum_{i=1}^N |\phi_i(\vec{r})|^2$ is expressible in terms of the N auxiliary

single-particle wave functions $\phi_i(\vec{r})$ of lowest energy from the Kohn-Sham equations

$$\left[-\frac{1}{2m_e}\Delta + V_{ion} + \int d\mathbf{r}' V_{ee}n(\mathbf{r}') + \frac{\delta E_{xc}[n]}{\delta n} \right] \phi_i(\vec{r}) = \epsilon_i \phi_i(\vec{r}), \quad (2.6)$$

which are obtained by varying Eq.(2.3) w.r.t. ϕ_i and fixed N . This allows us to use the effective single-particle wave functions ϕ_i in an iterative minimization procedure to find the electron density consistent with the Kohn-Sham equations.

There are, however, material classes where the LDA is inappropriate and leads to qualitatively wrong predictions. These are typically materials with partially filled d or f shells, where two electrons may occupy one of the narrow orbitals on the same lattice site and correlation effects become non-negligible.

Lattice models. A different approach to the many-body problem for electrons is to start with a model Hamiltonian, rather than using the complicated ab initio Hamiltonian from Eq.(2.1). The intention is to restrict the model to a parametric description of the very essential mechanisms only, namely the electron hopping from one lattice site to another and the Coulomb interaction which is assumed to be strongly screened and therefore purely local. A general form of such a lattice model Hamiltonian may be written as follows:

$$H = - \sum_{ijl\sigma} t_{ij} c_{il\sigma}^\dagger c_{jl\sigma} + \sum_{ilmno\sigma\sigma'} U_{lmno} c_{il\sigma}^\dagger c_{im\sigma} c_{in\sigma'}^\dagger c_{io\sigma'}. \quad (2.7)$$

Here $c_{il\sigma}^\dagger$ and $c_{il\sigma}$ are operators creating and annihilating an electron, with the indices i , l and σ for lattice site, orbital and spin, correspondingly; t_{ij} denotes the hopping amplitude between the lattice sites i and j ; U_{lmno} are the parameters accounting for the local Coulomb interaction. Probably the most prominent representative is the single-band Hubbard model:

$$H = -t \sum_{\langle i,j \rangle \sigma} c_{i\sigma}^\dagger c_{j\sigma} + U \sum_i n_{i\uparrow} n_{i\downarrow}, \quad (2.8)$$

which was in 1963 proposed independently by J. Hubbard [4], M.C. Gutzwiller [5] and J. Kanamori [6]. In the Hamiltonian of Eq.(2.8) the hopping is restricted to the nearest neighbor sites $\langle i, j \rangle$ and each lattice site can be occupied at most by two electrons of opposite spin, thus the model is characterized by just two parameters t and U . Although the model gives a

simple impression, there only exist analytical solutions in one dimension and a numerical exact approach in infinite dimensions, namely dynamical mean-field theory, which we discuss in the third chapter.

In summary, LDA is inappropriate to account for many-body effects originating from strong electronic correlation. In this case DMFT gives a good description of the local dynamics. In Chap. 3 we will see that solving a lattice model in DMFT essentially amounts to finding a self-consistent solution of an impurity model. Therefore we start with a description of such quantum impurity models in the first section of this chapter.

The solution of an impurity model is usually expressed in terms of many-particle Green's functions. We will define them and develop some of their analytic properties in the subsequent section.

2.1 Quantum Impurity Models

A quantum impurity model represents an atom in a host medium with which it can exchange electrons. The impurity is typically characterized by a small number of discrete degrees of freedom, whereas the host medium or bath is represented by a non-interacting infinite system with a continuous spectrum. The Hamiltonian of a multi-band impurity model may be written in the following form:

$$\begin{aligned}
 H = & \underbrace{\mu \sum_{\alpha} c_{\alpha}^{\dagger} c_{\alpha}}_{H_{loc}^0} + \underbrace{\sum_{\alpha\beta\gamma\delta} U^{\alpha\beta\gamma\delta} c_{\alpha}^{\dagger} c_{\beta} c_{\gamma}^{\dagger} c_{\delta}}_{H_{loc}^I} + \\
 & + \underbrace{\sum_{k,\alpha} \epsilon_k a_{k\alpha}^{\dagger} a_{k\alpha}}_{H_{bath}} + \underbrace{\sum_{k,\alpha} \left(V_k^{\alpha} a_{k\alpha}^{\dagger} c_{\alpha} + h.c. \right)}_{H_{hyb}},
 \end{aligned} \tag{2.9}$$

where c_{α}^{\dagger} (c_{α}) denote creation (annihilation) operators of electrons on the impurity site characterized by the combined¹ spin and band index α . These electrons are correlated via the local interaction $U^{\alpha\beta\gamma\delta}$. The chemical potential μ accounts for the level energy. The terms containing only the impurity operators are combined in the local Hamiltonians H_{loc}^I and H_{loc}^0 , where the superscripts stand for the interacting and non-interacting part, correspondingly. The operators $a_{k\alpha}^{\dagger}$ ($a_{k\alpha}$) create (annihilate) states with momentum k and combined spin-band index α . The band energy of these

¹In order to avoid cluttering up the notation unnecessarily we write a single index on operators like c_{α} when we actually mean $c_{l\sigma}$ with l and σ denoting the indices for band and spin correspondingly.

uncorrelated bath states is given by the dispersion relation ϵ_k . The terms containing only the bath operators are collected in the bath Hamiltonian H_{bath} . The mixed terms, characterized by the hybridization matrix V_k^α , account for the electron hopping from the impurity into the bath and vice versa. These are contained in H_{hyb} which we have here chosen to be block-diagonal in α , although more complicated mixing terms may be considered as well.

Single Impurity Anderson Model (SIAM). Obviously the simplest, non-trivial, special case of Eq.(2.9) is to allow only for a single orbital, such that the local interaction simplifies drastically:

$$H = \mu \sum_{\sigma} n_{\sigma} + U n_{\uparrow} n_{\downarrow} + \sum_{k,\sigma} \epsilon_k a_{k\sigma}^{\dagger} a_{k\sigma} + \sum_{k,\sigma} \left(V_k^{\sigma} a_{k\sigma}^{\dagger} c_{\sigma} + h.c. \right). \quad (2.10)$$

The interaction matrix simplifies to a single number U and the multi-index is reduced to a spin index σ . This Hamiltonian was first proposed by Anderson [7] in 1961 who used it to describe the properties of magnetic impurities in a non-magnetic host metal.

Slater-Kanamori Model. A more sophisticated choice, involving several correlated bands, is the Slater-Kanamori model [8, 9] where the local Hamiltonian is given by:

$$\begin{aligned} H_{loc}^I = & \sum_a U n_{a\uparrow} n_{a\downarrow} + \sum_{a>b,\sigma} [U' n_{a\sigma} n_{a\bar{\sigma}} + (U' - J) n_{a\sigma} n_{b\sigma}] \\ & - \sum_{a \neq b} J \left(c_{a\downarrow}^{\dagger} c_{b\uparrow}^{\dagger} c_{b\downarrow} c_{a\uparrow} + c_{b\downarrow}^{\dagger} c_{b\uparrow}^{\dagger} c_{a\downarrow} c_{a\uparrow} + h.c. \right). \end{aligned} \quad (2.11)$$

Above, U and U' denote the intra- and inter-orbital Coulomb interaction, respectively. The exchange coefficient J , taking Hund coupling into account, with U' chosen such that $U' = U - 2J$. The Slater-Kanamori Hamiltonian is chosen such that the operator combination in the Hund term is SU(2) symmetric, i.e. it is invariant under rotations in spin space. It is, however, not diagonal in spin-band space. In the Hamiltonian of Eq.(2.11) only scattering events between equal and different orbitals are distinguished, but it makes no difference which orbitals are involved, resulting in a rather high degeneracy of the different energy levels (see Figure 2.1).

Spherical Symmetric Coulomb Model. It is also possible to use the 'true' $1/r$ potential to model the local interaction. Therefore we employ

the scattering amplitudes associated with the spherical symmetric Coulomb potential represented in an eigenbasis of the central field problem. This results, compared to the Kanamori interaction, in a much less degenerated eigenvalue spectrum (see Figure 2.1). The local Hamiltonian, which we derive in detail in Appendix A.3, becomes:

$$H_{loc}^I = \sum_{mnpq\sigma\sigma'} \delta_{m+n,p+q} (-1)^{m+p} (2l-1)^2 c_{m\sigma}^\dagger c_{n\sigma'}^\dagger c_{p\sigma} c_{q\sigma'} \times \sum_{k=0}^{2l} \begin{pmatrix} l & l & k \\ 0 & 0 & 0 \end{pmatrix}^2 \begin{pmatrix} l & l & k \\ -m & p & m-p \end{pmatrix} \begin{pmatrix} l & l & k \\ -n & q & n-q \end{pmatrix} R_k. \quad (2.12)$$

The angular dependent part is analytically expressible in terms of Wigner 3-j symbols $\begin{pmatrix} a & b & c \\ d & e & f \end{pmatrix}$ (see Appendix A.1). The remaining radial part R_k , known as Slater integrals, become parameters of the Hamiltonian which describes the interaction in a shell denoted by the angular momentum quantum number l . As we show in Appendix A.3, the sum index $k \leq 2l$ has to run over even values only. The band index m of an operator $c_{m\sigma}$ is assigned to the quantum number associated with the z-component of the angular momentum operator and is therefore restricted by the condition $-l \leq m \leq l$. Hence, only models with 1,3,5,... orbitals are compatible with this kind of local interaction, and 2,4,6,... orbitals are not allowed. The simplest Coulomb model, different from the SIAM, is therefore one with three bands. The interaction distinguishes between particular bands and the number of required parameters R_k depends on the number of bands taken into account.

2.2 Finite Temperature Green's Functions

In the context of many-particle quantum mechanics a n -particle Green's function, or $2n$ -point function, may be defined as follows:

$$G_{\alpha_1\alpha'_1\ldots\alpha_n\alpha'_n}^{(n)}(t_1, t'_1, \ldots, t_n, t'_n) = (-i)^n \langle T c_{\alpha_1}(t_1) c_{\alpha'_1}^\dagger(t'_1) \ldots c_{\alpha_n}(t_n) c_{\alpha'_n}^\dagger(t'_n) \rangle. \quad (2.13)$$

The operators are given in Heisenberg representation:

$$\begin{aligned} c_\alpha(t) &:= e^{itH} c_\alpha e^{-itH}, \\ c_\alpha^\dagger(t) &:= e^{itH} c_\alpha^\dagger e^{-itH}. \end{aligned} \quad (2.14)$$

The combined index α contains a spin index σ and may contain other indices, e.g., for a discrete energy level a and a site index i taking the

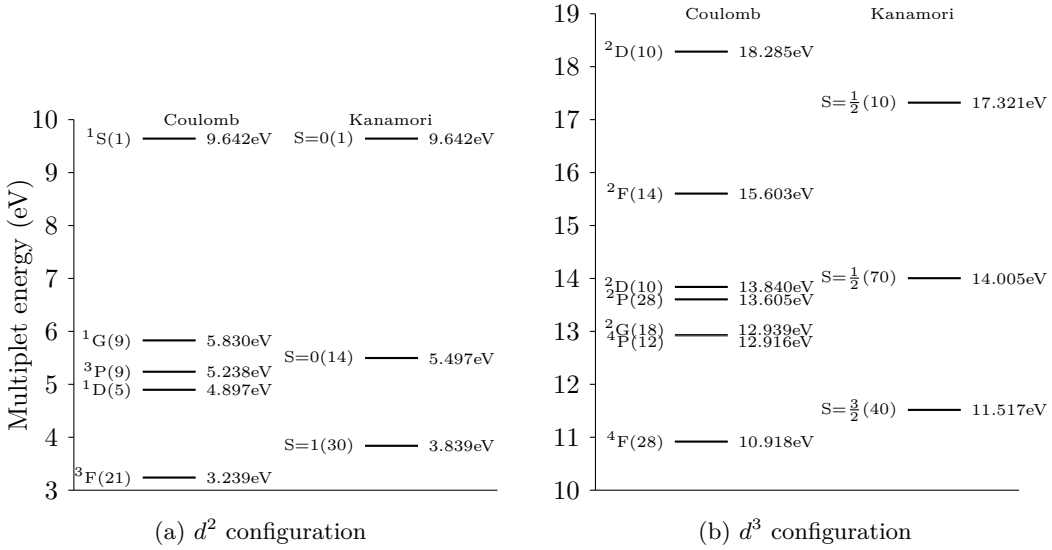


Figure 2.1: Energy levels of (a) d^2 and (b) d^3 configuration. All states having the same number of electrons and angular momentum quantum number are said to belong to the same configuration. A d^2 configuration, for example, denotes a d -orbital occupied with 2 electrons. The energy levels of the Coulomb model are labeled according to the Russell-Saunders term scheme: ^{2S+1}L . For the Kanamori levels the total spin serves as label. The degeneracy is written in parentheses beside the term name. Compared to the Kanamori model, the degeneracy of several energy levels is lifted in the Coulomb model.

discrete spacial dependence on a lattice into account:

$$c_\alpha(t) = c_{i\sigma\alpha}(t). \quad (2.15)$$

The thermal expectation value is defined as:

$$\langle \dots \rangle = \frac{1}{Z} \text{Tr} \left(e^{-\beta H} \dots \right) \quad (2.16)$$

with the partition function Z given by:

$$Z = \text{Tr} e^{-\beta H}, \quad (2.17)$$

and the inverse temperature $\beta = \frac{1}{T}$. For operators $A(t_1)$, $B(t_2)$ which obey the fermionic anti-commutation relations, the time-ordering symbol T that appears in Eq.(2.13) is defined as:

$$TA(t_1)B(t_2) = \begin{cases} A(t_1)B(t_2) & \forall t_1 > t_2 \\ -B(t_2)A(t_1) & \forall t_2 > t_1. \end{cases} \quad (2.18)$$

In the single-particle case ($n = 1$) the Green's function has the physical interpretation of a transition amplitude of an additional electron that is added to the system at time t_1 and removed at t_2 when $t_1 < t_2$. For $t_1 > t_2$ it describes the propagation of a hole.

At finite temperature a formulation in imaginary time rather than real time turns out to be favorable. This can be seen by comparing the Boltzmann weight appearing in Eq.(2.17) with the exponentials of time evolution in Eq.(2.14):

$$e^{-\frac{H}{T}} \rightarrow e^{-\beta H}, \quad e^{itH} \rightarrow e^{-\tau H}. \quad (2.19)$$

The formal equivalence of inverse temperature β and imaginary time $\tau \equiv -it$, motivates the following Heisenberg like operator representation:

$$\begin{aligned} c_\alpha(\tau) &:= e^{\tau H} c_\alpha e^{-H\tau}, \\ c_\alpha^\dagger(\tau) &:= e^{\tau H} c_\alpha^\dagger e^{-H\tau}, \end{aligned} \quad (2.20)$$

which allows to treat the Boltzmann factor and the now imaginary time evolution on equal footings. It is important to note that the conjugate imaginary time operator $c_\alpha^\dagger(\tau)$ is not the hermitian conjugate of $c_\alpha(\tau)$:

$$\begin{aligned} c_\alpha^\dagger(\tau) &= (e^{\tau H} c_\alpha e^{-H\tau})^\dagger \\ &= e^{-H\tau} c_\alpha^\dagger e^{\tau H} \neq c_\alpha^\dagger(\tau). \end{aligned} \quad (2.21)$$

We define the n -particle imaginary time Green's function as follows:

$$G_{\alpha_1\alpha'_1\dots\alpha_n\alpha'_n}^{(n)}(\tau_1, \tau'_1, \dots, \tau_n, \tau'_n) = (-1)^n \langle T_\tau c_{\alpha_1}(\tau_1) c_{\alpha'_1}^\dagger(\tau'_1) \dots c_{\alpha_n}(\tau_n) c_{\alpha'_n}^\dagger(\tau'_n) \rangle, \quad (2.22)$$

where the definition of the ordering symbol T_τ is analogous to that of T in Eq.(2.18).

Single-Particle Green's Function. A fundamental quantity in describing quantum mechanical many-body systems is the single-particle Green's function as it accounts for the propagation of the excitations in the system. In accordance to Eq.(2.22) the finite temperature single-particle Green's function is given by:

$$G_{\alpha\beta}(\tau_1, \tau_2) := - \langle T_\tau c_\alpha(\tau_1) c_\beta^\dagger(\tau_2) \rangle. \quad (2.23)$$

For Hamiltonians without explicit time dependence the Green's function is translational invariant in τ :

$$\begin{aligned} G_{\alpha\beta}(\tau_1, \tau_2) &= -\frac{1}{Z} \text{Tr} \left(e^{-\beta H} T_\tau c_\alpha(\tau_1) c_\beta^\dagger(\tau_2) \right) \\ &= -\frac{1}{Z} \left[\text{Tr} \left(e^{-\beta H} e^{\tau_1 H} c_\alpha e^{-\tau_1 H} e^{\tau_2 H} c_\beta^\dagger e^{-\tau_2 H} \right) \theta(\tau_1 - \tau_2) \right. \\ &\quad \left. - \text{Tr} \left(e^{-\beta H} e^{\tau_2 H} c_\beta^\dagger e^{-\tau_2 H} e^{\tau_1 H} c_\alpha e^{-\tau_1 H} \right) \theta(\tau_2 - \tau_1) \right] \\ &= -\frac{1}{Z} \left[\text{Tr} \left(e^{-\beta H} e^{(\tau_1 - \tau_2) H} c_\alpha e^{-(\tau_1 - \tau_2) H} c_\beta^\dagger \right) \theta(\tau_1 - \tau_2) \right. \\ &\quad \left. - \text{Tr} \left(e^{-\beta H} c_\beta^\dagger e^{(\tau_1 - \tau_2) H} c_\alpha e^{-(\tau_1 - \tau_2) H} \right) \theta(\tau_2 - \tau_1) \right] \\ &= G_{\alpha\beta}(\tau_1 - \tau_2, 0) \equiv G_{\alpha\beta}(\tau). \end{aligned} \quad (2.24)$$

We have employed the cyclic property of the trace and the θ -functions implement the time ordering T_τ .

As a next step we show that the single-particle Green's function is anti-periodic, and thus can be written in terms of a Fourier series. For this purpose we first evaluate the trace Eq.(2.24), using a complete set of energy eigenstates $\{|n\rangle\}$:

$$\begin{aligned} G_{\alpha\beta}(\tau) &= -\frac{1}{Z} \sum_n [e^{-(\beta - \tau)E_n} \langle n | c_\alpha e^{-\tau H} c_\beta^\dagger | n \rangle \theta(\tau) \\ &\quad - e^{-(\beta + \tau)E_n} \langle n | c_\beta^\dagger e^{\tau H} c_\alpha | n \rangle \theta(-\tau)]. \end{aligned} \quad (2.25)$$

For an infinite system the spectrum is unbounded from above and the sum in Eq.(2.25) only converges if τ is restricted to the finite range:

$$\tau \in [-\beta, \beta], \quad (2.26)$$

such that contributions corresponding to large values of E_n are exponentially damped. To prove the anti-periodicity, we take a closer look at the explicit expression for $G(\tau + \beta)$ in the case where $\tau < 0$:

$$\begin{aligned}
 G_{\alpha\beta}(\tau + \beta) &= -\frac{1}{Z} \text{Tr} \left(e^{-\beta H} e^{(\tau+\beta)H} c_\alpha e^{-(\tau+\beta)H} c_\beta^\dagger \right) \\
 &= -\frac{1}{Z} \text{Tr} \left(e^{\tau H} c_\alpha e^{-(\tau+\beta)H} c_\beta^\dagger \right) \\
 &= -\frac{1}{Z} \text{Tr} \left(e^{-\beta H} c_\beta^\dagger e^{\tau H} c_\alpha e^{-\tau H} \right) \\
 &= -G_{\alpha\beta}(\tau).
 \end{aligned} \tag{2.27}$$

By using again the cyclic property of the trace we obtain the important result that the Green's function is anti-periodic with period β and can therefore be expressed as Fourier series:

$$G_{\alpha\beta}(\tau) = \frac{1}{\beta} \sum_{n=-\infty}^{\infty} e^{-i\nu_n \tau} G_{\alpha\beta}(i\nu_n). \tag{2.28}$$

Due to the anti-periodicity of $G_{\alpha\beta}(\tau)$ the series must involve only odd Matsubara frequencies:

$$\nu_n = \frac{(2n+1)\pi}{\beta} \quad \text{with } n \in \mathbb{Z}. \tag{2.29}$$

The Fourier coefficients $G_{\alpha\beta}(i\nu_n)$ are given by the inverse transformation:

$$G_{\alpha\beta}(i\nu_n) = \int_0^\beta d\tau e^{i\nu_n \tau} G_{\alpha\beta}(\tau). \tag{2.30}$$

At $\tau = 0$ the single-particle Green's function is discontinuous. Using the linear property of the trace we can calculate the jump size ΔG of the discontinuity:

$$\begin{aligned}
 \Delta G &\equiv \lim_{\tau \rightarrow +0} \left(G_{\alpha\beta}(\tau) - G_{\alpha\beta}(-\tau) \right) \\
 &= \langle c_\alpha c_\beta^\dagger \rangle + \langle c_\beta^\dagger c_\alpha \rangle \\
 &= \langle \{c_\alpha, c_\beta^\dagger\} \rangle = \delta_{\alpha\beta}.
 \end{aligned} \tag{2.31}$$

As we will see, this discontinuity translates into a corresponding discontinuity of the two-particle Green's function. In Figure 2.2 we illustrate some of the analytical features of the single-particle Green's function for the example of the Hubbard model.

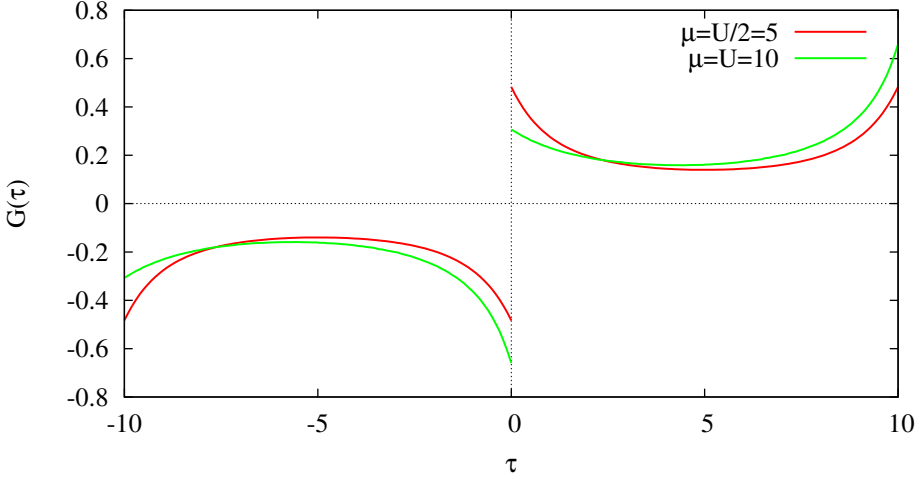


Figure 2.2: Single-particle Green's function of the Hubbard model given in Eq.(2.8) on an infinite dimensional Bethe lattice, for $\beta = 10$, at half and non-half filling. At half filling ($\mu = U/2$) the Green's function has, in addition to the anti-periodicity, on $[0, \beta]$ a symmetry around $\beta/2$. In both cases there is a discontinuity of amplitude one at $\tau = 0$.

Two-Particle Green's Function. According to Eq.(2.22) the two-particle Green's function is defined as:

$$G_{\alpha}(\tau_1, \tau_2, \tau_3, \tau_4) := \left\langle T_{\tau} c_{\alpha_1}(\tau_1) c_{\alpha_2}^+(\tau_2) c_{\alpha_3}(\tau_3) c_{\alpha_4}^+(\tau_4) \right\rangle. \quad (2.32)$$

Due to the same arguments as for the single-particle Green's function the two-particle Green's function is translational invariant in all four τ arguments, which allows to set one argument to zero. We choose to subtract τ_4 from each τ_i and change the indices ($\tau_i - \tau_4 \rightarrow \tau_i$) which results in:

$$G_{\alpha}(\tau_1, \tau_2, \tau_3) := \left\langle T_{\tau} c_{\alpha_1}(\tau_1) c_{\alpha_2}^+(\tau_2) c_{\alpha_3}(\tau_3) c_{\alpha_4}^{\dagger} \right\rangle. \quad (2.33)$$

The two-particle Green's function is β anti-periodic in each argument:

$$G_{\alpha}(\dots, \tau_i, \dots) = -G_{\alpha}(\dots, \tau_i - \beta, \dots), \quad (2.34)$$

with the restriction:

$$\tau_i \in [-\beta, \beta]. \quad (2.35)$$

The Fourier expansion in terms of Matsubara frequencies reads:

$$G_{\alpha}(\tau_1, \tau_2, \tau_3) = \frac{1}{\beta^3} \sum_{\{\nu_i\}} e^{-i(\nu_1 \tau_1 - \nu_2 \tau_2 + \nu_3 \tau_3)} G_{\alpha}(\nu_1, \nu_2, \nu_3). \quad (2.36)$$

The Fourier coefficients are obtained by the inverse transformation:

$$G_{\alpha}(\nu_1, \nu_2, \nu_3) = \int_0^{\beta} d\tau_1 \int_0^{\beta} d\tau_2 \int_0^{\beta} d\tau_3 e^{i(\nu_1\tau_1 - \nu_2\tau_2 + \nu_3\tau_3)} G_{\alpha}(\tau_1, \tau_2, \tau_3). \quad (2.37)$$

If any two τ 's are equal, the two-particle Green's function has a discontinuity. We demonstrate this for the special case where $\tau \equiv \tau_1 = \tau_2 > \tau_3 > 0$ with some $\epsilon > 0$:

$$\begin{aligned} \Delta G_{\alpha}(\tau_3) &\equiv \lim_{\epsilon \rightarrow 0} \left(G_{\alpha}(\tau + \epsilon, \tau, \tau_3) - G_{\alpha}(\tau - \epsilon, \tau, \tau_3) \right) \\ &= \lim_{\epsilon \rightarrow 0} \left(\langle c_{\alpha_1}(\tau + \epsilon) c_{\alpha_2}^+(\tau) c_{\alpha_3}(\tau_3) c_{\alpha_4}^+ \rangle + \langle c_{\alpha_2}^+(\tau) c_{\alpha_1}(\tau - \epsilon) c_{\alpha_3}(\tau_3) c_{\alpha_4}^+ \rangle \right) \\ &= \langle e^{H\tau} c_{\alpha_1} c_{\alpha_2}^+ e^{-H\tau} c_{\alpha_3}(\tau_3) c_{\alpha_4}^+ \rangle + \langle e^{H\tau} c_{\alpha_2}^+ c_{\alpha_1} e^{-H\tau} c_{\alpha_3}(\tau_3) c_{\alpha_4}^+ \rangle \\ &= \langle e^{H\tau} c_{\alpha_1} c_{\alpha_2}^+ e^{-H\tau} c_{\alpha_3}(\tau_3) c_{\alpha_4}^+ \rangle + \langle e^{H\tau} (\delta_{\alpha_1\alpha_2} - c_{\alpha_1} c_{\alpha_2}^+) e^{-H\tau} c_{\alpha_3}(\tau_3) c_{\alpha_4}^+ \rangle \\ &= \delta_{\alpha_1\alpha_2} \langle c_{\alpha_3}(\tau_3) c_{\alpha_4}^+ \rangle \end{aligned} \quad (2.38)$$

Because of the implicit time ordering the second term in the second line changes sign. In the fourth line we used the fermionic equal time anti-commutation relation: $\{c_{\alpha_1}, c_{\alpha_2}^+\} = \delta_{\alpha_1\alpha_2}$.

It is easy to show that this discontinuity comes entirely from the disconnected part of the full Green's function, i.e. it is inherited from the single-particle Green's function. The disconnected part $D_{\alpha}(\tau_1, \tau_2, \tau_3)$ of the full two-particle Green's function is defined as:

$$\begin{aligned} D_{\alpha}(\tau_1, \tau_2, \tau_3) &:= \langle T_{\tau} \overbrace{c_{\alpha_1}(\tau_1) c_{\alpha_2}^+(\tau_2)}^{\text{connected}} \overbrace{c_{\alpha_3}(\tau_3) c_{\alpha_4}^+}^{\text{connected}} \rangle \\ &= G_{\alpha_1\alpha_2}(\tau_1 - \tau_2) G_{\alpha_3\alpha_4}(\tau_3) - G_{\alpha_1\alpha_4}(\tau_1) G_{\alpha_3\alpha_2}(\tau_3 - \tau_2) \end{aligned} \quad (2.39)$$

Again we look at the special case where $\tau \equiv \tau_1 = \tau_2 > \tau_3 > 0$ with $\epsilon > 0$:

$$\begin{aligned} \Delta D_{\alpha}(\tau_3) &\equiv \lim_{\epsilon \rightarrow 0} \left(D_{\alpha}(\tau + \epsilon, \tau, \tau_3) - D_{\alpha}(\tau - \epsilon, \tau, \tau_3) \right) \\ &= \lim_{\epsilon \rightarrow 0} \left(\langle c_{\alpha_1}(\tau + \epsilon) c_{\alpha_2}^+(\tau) \rangle \langle c_{\alpha_3}(\tau_3) c_{\alpha_4}^+ \rangle + \langle c_{\alpha_1}(\tau + \epsilon) c_{\alpha_4}^+ \rangle \langle c_{\alpha_2}^+(\tau) c_{\alpha_3}(\tau_3) \rangle \right. \\ &\quad \left. + \langle c_{\alpha_2}^+(\tau) c_{\alpha_1}(\tau - \epsilon) \rangle \langle c_{\alpha_3}(\tau_3) c_{\alpha_4}^+ \rangle - \langle c_{\alpha_1}(\tau - \epsilon) c_{\alpha_4}^+ \rangle \langle c_{\alpha_2}^+(\tau) c_{\alpha_3}(\tau_3) \rangle \right) \\ &= \delta_{\alpha_1\alpha_2} \langle c_{\alpha_3}(\tau_3) c_{\alpha_4}^+ \rangle \end{aligned} \quad (2.40)$$

The result for $\Delta D_\alpha(\tau_3)$ is exactly what we found for the case of the full Green's function $\Delta G_\alpha(\tau_3)$, so we conclude that the discontinuity is entirely inherited from the disconnected part and the fully connected part is therefore continuous. The above example demonstrates that the step size includes a Kronecker delta originating from the anti-commutation relations between the operators with equal values of τ_i . This immediately makes clear that there is no discontinuity when the corresponding anti-commutator vanishes. With the knowledge that the single-particle Green's function makes a jump at $\tau = 0$, the discontinuity structure of $\Delta G_\alpha(\tau_3)$ is manifest. The two-particle Green's function has a discontinuity when the argument of any single-particle Green's function in $D_\alpha(\tau_1, \tau_2, \tau_3)$ vanishes. Deriving the results for all other combinations works in complete analogy as above.

For the paramagnetic², single-orbital case with conservation of total spin the indices on the two-particle Green's function reduce to:

$$G_{\sigma\sigma'}(\tau_1, \tau_2, \tau_3) = \langle T_\tau c_\sigma(\tau_1) c_\sigma^+(\tau_2) c_{\sigma'}(\tau_3) c_{\sigma'}^+ \rangle. \quad (2.41)$$

The Generalized Susceptibility. A quantity closely related to the two-particle Green's function is the generalized susceptibility:

$$\begin{aligned} \chi_\alpha(\tau_1, \tau_2, \tau_3, \tau_4) &\equiv \langle T_\tau c_{\alpha_1}^+(\tau_1) c_{\alpha_2}(\tau_2) c_{\alpha_3}^+(\tau_3) c_{\alpha_4}(\tau_4) \rangle \\ &\quad - \langle T_\tau c_{\alpha_1}^+(\tau_1) c_{\alpha_2}(\tau_2) \rangle \langle T_\tau c_{\alpha_3}^+(\tau_3) c_{\alpha_4}(\tau_4) \rangle \\ &= G_\alpha(\tau_1, \tau_2, \tau_3, \tau_4) - G_{\alpha_1\alpha_2}(\tau_1, \tau_2) G_{\alpha_3\alpha_4}(\tau_3, 0) \end{aligned} \quad (2.42)$$

We restrict our discussion to the single-band case, where due to time translational symmetry, SU(2)-symmetry and crossing symmetry (for details see [10]) the generalized susceptibility takes the simpler form:

$$\chi_{\sigma\sigma'}(\tau_1, \tau_2, \tau_3) \equiv G_{\sigma\sigma'}(\tau_1, \tau_2, \tau_3) - G_\sigma(\tau_1, \tau_2) G_{\sigma'}(\tau_3, 0). \quad (2.43)$$

The transformation to frequency representation may be defined in two different ways, referred to as particle-hole (*ph*) and particle-particle (*pp*) representation:

$$\chi_{ph,\sigma\sigma'}^{\nu\nu'\omega} := \int_0^\beta d\tau_1 \int_0^\beta d\tau_2 \int_0^\beta d\tau_3 e^{-i\nu\tau_1} e^{i(\nu+\omega)\tau_2} e^{-i(\nu'+\omega)\tau_3} \chi_{\sigma\sigma'}(\tau_1, \tau_2, \tau_3), \quad (2.44)$$

²Flipping all spins simultaneously leaves the system unchanged.

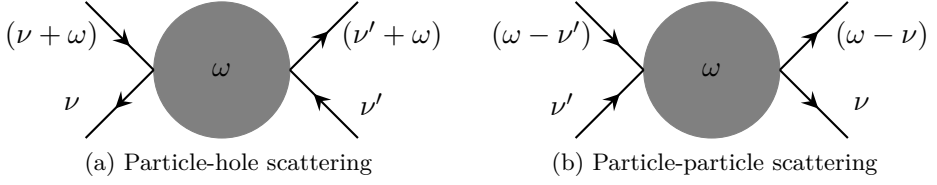


Figure 2.3: The particle-hole case (a) corresponds to the scattering process between a hole of energy $-\nu$ and an electron of energy $\omega + \nu$. The particle-particle case (b) corresponds to a scattering process between two electrons with energy ν' and $\omega - \nu'$. In both processes the total energy of ω is transferred (this figure is adopted from [10]).

$$\chi_{pp,\sigma\sigma'}^{\nu\nu'\omega} := \int_0^\beta d\tau_1 \int_0^\beta d\tau_2 \int_0^\beta d\tau_3 e^{-i\nu\tau_1} e^{i(\omega-\nu')\tau_2} e^{-i(\omega-\nu)\tau_3} \chi_{\sigma\sigma'}(\tau_1, \tau_2, \tau_3), \quad (2.45)$$

where ν and ν' are fermionic Matsubara frequencies ($\nu, \nu' = \frac{\pi}{\beta}(2n+1), n \in \mathbb{Z}$) and ω denotes a bosonic Matsubara frequency ($\omega = \frac{2n\pi}{\beta}, n \in \mathbb{Z}$). The physical motivation behind these two frequency conventions is discussed in Figure 2.3. Comparing the exponentials in Eq.(2.44) and Eq.(2.45) makes clear that χ_{pp} can be obtained from χ_{ph} by a mere frequency shift in ω :

$$\chi_{pp,\sigma\sigma'}^{\nu\nu'\omega} = \chi_{ph,\sigma\sigma'}^{\nu\nu'(\omega-\nu-\nu')}. \quad (2.46)$$

Chapter 3

Dynamical Mean-Field Theory

The standard approach to get approximate solutions of quantum mechanical lattice models is to employ a perturbative expansion around an analytically tractable limit. In the Hubbard Hamiltonian of Eq.(2.8) two such limits are manifest, namely the atomic limit, where the hopping parameter t is assumed to be small compared to the local interaction U and perturbation theory in t applies around $t = 0$, and the opposite case, the free limit, where U is assumed to be small compared to t and a perturbative expansion in U is applicable around $U = 0$. However, neither of both limits is justified if the energy scales of kinetic and interaction energy are of the same order of magnitude. But it is just the equivalence of these energy scales, which makes a non-trivial interplay between itinerancy and localization of the electrons possible and gives in turn rise to such interesting many-body effects like Mott insulation. Therefore Metzner and Vollhardt [11] introduced the limit of infinite dimensions as an alternative. In this limit the inverse dimension of space serves as small parameter. A proper rescaling of the lattice Hamiltonian results in a non-trivial limit without making any *a priori* assumptions about the relative size of U and t . This makes parameter regions accessible where U and t are on the same energy scale. Müller-Hartmann [12] showed that in the limit of infinite dimensions the self-energy becomes purely local which results in a tremendous reduction in the variety of non-vanishing contributions in its diagrammatic expansion. This in turn allows to reduce the lattice model to an effective impurity model which needs to be solved self-consistently, such that its interaction with the effective bath is equivalent to the dynamics of the underlying lattice model. This amounts to a huge decrease of complexity, since there

exist numerical exact methods, like Quantum Monte Carlo algorithms, to obtain solutions of impurity models.

3.1 The Limit of Infinite Dimensions

Let us start with analyzing the scaling of the Hubbard Hamiltonian Eq.(2.8) in the limit of $d \rightarrow \infty$. We restrict the following discussion to the paramagnetic¹, single-band case which is sufficient to demonstrate the essential steps without cluttering up the notation. The generalization to the multi-orbital lattice Hamiltonian of Eq.(2.7) is straight forward. Since the lattice Hamiltonian includes a sum over neighboring lattice sites, it is convenient to introduce the coordination number Z of neighbor sites. Z is completely defined by the lattice type and the number of dimensions and we can (and will) use $\frac{1}{Z}$ instead of $\frac{1}{d}$ as the small parameter. In that way we avoid the need of referring to a specific lattice type. For the Hubbard Hamiltonian, which is restricted to nearest neighbor hopping only, Z is given by the number of nearest neighbor sites. In the case of a bcc lattice in 3 dimensions, for example, $Z = 8$. We will now argue diagrammatically how to rescale the Hamiltonian in terms of Z to get a non-trivial limit for $Z \rightarrow \infty$ (or equiv. $d \rightarrow \infty$).

Renormalization of the Lattice Hamiltonian. First we take a look at the local interaction term. This contribution is obviously independent of the lattice type and the number of dimensions, hence its thermal expectation value does not scale with Z and stays, without any modifications, finite in the limit of $Z \rightarrow \infty$:

$$\lim_{Z \rightarrow \infty} \left\langle U \sum_i n_{i\uparrow} n_{i\downarrow} \right\rangle = \text{const.} \quad (3.1)$$

The scaling of the hopping term, on the other hand, is non-trivial:

$$\lim_{Z \rightarrow \infty} \left\langle t \sum_{\langle i,j \rangle \sigma} c_{i\sigma}^\dagger c_{j\sigma} \right\rangle = \left\langle tZ \sum_{\sigma} c_{i\sigma}^\dagger c_{j\sigma} \middle| \right\rangle_{\langle i,j \rangle} = \infty. \quad (3.2)$$

The sum over the nearest neighbor sites gives an overall factor of Z and the expectation value hence diverges. In order to avoid the above divergence and to obtain a non-zero expectation value we need to renormalize the hopping amplitude t properly. Our strategy is to postulate the following scaling:

$$t = \frac{t^*}{\sqrt{Z}}, \quad (3.3)$$

¹In the paramagnetic phase $G_\downarrow = G_\uparrow$ holds, so that we can omit the spin index.

with $t^* = \text{const.}$, and to show *a posteriori* that our assumption is correct. First, we notice that the hopping term, that controls the electron propagation between the lattice sites, is closely related to the single-particle propagator:

$$G_{ij}(0+) = \langle c_i c_j^\dagger \rangle = \delta_{ij} - \langle c_i^\dagger c_j \rangle. \quad (3.4)$$

We have used the definition Eq.(2.23) and the fermionic equal time anti-commutation relation $\{c_i, c_j^\dagger\} = \delta_{ij}$. The propagator $G_{ij}(i\omega_n)$ should better scale as $\frac{1}{\sqrt{Z}}$ in order to compensate in combination with the rescaled t the factor Z from the summation. To see that this is indeed the case, we first express G in terms of the bare propagator G_0 and the self-energy Σ using Dyson's equation:

$$G_{ij}^{-1}(i\omega_n) = [G_{ij}^0(i\omega_n)]^{-1} - \Sigma_{ij}(i\omega_n). \quad (3.5)$$

We are now left over with the task of determining the scaling properties of G_0 and Σ . We derive the required formula for the free propagator G^0 in Appendix B.1 and rewrite it here as:

$$G_{ij}^0(i\omega_n) = [\delta_{ij}(i\omega_n + t) - t]_{ij}^{-1}. \quad (3.6)$$

Using the following matrix identity:

$$A^{-1} = \frac{1}{\det A} \text{adj} A \quad (3.7)$$

and looking at the simple case of two lattice sites where the matrix inverse is easily obtained:

$$G_{ij}^0(i\omega_n) = \begin{pmatrix} i\omega_n & -t \\ -t & i\omega_n \end{pmatrix}^{-1} = \frac{1}{-\omega_n^2 - t^2} \begin{pmatrix} i\omega_n & t \\ t & i\omega_n \end{pmatrix} \quad (3.8)$$

we find for the off-diagonal terms:

$$\frac{t}{-\omega_n^2 - t^2} \propto \frac{Z^{-1/2}}{-1 - Z^{-1}} = \frac{1}{\sqrt{Z}} \frac{1}{-1 - \frac{1}{Z}}. \quad (3.9)$$

The factor $\frac{1}{-1 - \frac{1}{Z}}$ scales like a constant for large Z , and we find the following scaling for the bare propagator:

$$G_{ij}^0(i\omega_n) \propto \frac{1}{\sqrt{Z}}. \quad (3.10)$$

The same scaling holds for bigger matrices too as one can expect from Eq.(3.7). To get an idea of how the self-energy scales we employ a skeleton

expansion, meaning that we sum up all 1PI diagrams without external legs, with the internal bare propagators $G_{ij}^0(i\omega_n) = \frac{i}{\omega_n} \delta_{ij}$ replaced by fully dressed propagators $G_{ij}(i\omega_n) = \frac{i}{\omega_n} \delta_{ij}$. The local four point interaction is depicted as $U = \text{wavy line with four dots}$. Diagrammatically this may be written as follows:

$$\Sigma_{ij}(i\omega_n) = \text{bubble} + \text{bubble with wavy legs} + \dots + \text{bubble with wavy legs and internal loops} + \dots \quad (3.11)$$

We must not include diagrams like:

$$\text{bubble with wavy legs and top loop} = \text{bubble with wavy legs} + \text{bubble with wavy legs and bottom loop} + \dots + \text{bubble with wavy legs and multiple loops} + \dots \quad (3.12)$$

since they include additional self-energy contributions which would lead to a double counting of several diagrams. The following example should make this issue clear. Take, for instance, the second diagram on the r.h.s. of Eq.(3.11) and write it in terms of bare propagators:

$$\text{bubble with wavy legs} = \text{bubble} + \text{bubble with wavy legs} + \dots + \text{bubble with wavy legs and internal loops} + \dots \quad (3.13)$$

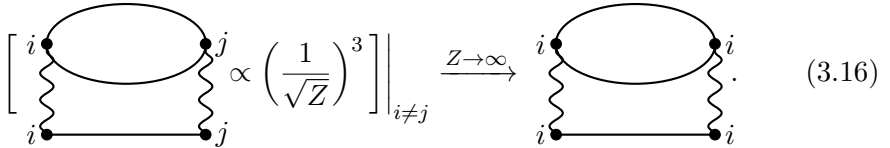
If we include diagrams like the one on the l.h.s. of Eq.(3.12) we would count several contributions twice, since the diagrams are already included in the propagator correction of the second diagram in the skeleton expansion given in Eq.(3.11). That is why we only include diagrams with internal loops connected with four legs to the rest. The diagrams having sub-diagrams which are connected with only two lines to the rest give additional self-energy contributions and must be excluded to avoid double counting. In the limit $Z \rightarrow \infty$, the scaling in Eq.(3.3) has the important consequence that the self-energy becomes a purely local quantity:

$$\Sigma_{ij}(i\omega_n) \xrightarrow{Z \rightarrow \infty} \delta_{ij} \Sigma_i(i\omega_n) \equiv \Sigma(i\omega_n), \quad (3.14)$$

or equivalently, after Fourier transformation, becomes momentum independent:

$$\Sigma(k, i\omega_n) \xrightarrow{Z \rightarrow \infty} \Sigma(\omega). \quad (3.15)$$

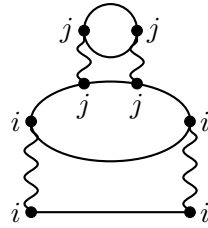
To better understand this important result we take a look at the first diagram on the r.h.s of Eq.(3.13) in the case where the three bare propagators have different site indices. We know that the bare propagators scale like $Z^{-1/2}$ resulting in an overall scaling of $Z^{-3/2}$, thus the contribution of the diagram vanishes for $Z \rightarrow \infty$, unless it becomes local i.e. $i = j$:



$$\left[\text{Diagram} \propto \left(\frac{1}{\sqrt{Z}} \right)^3 \right] \Big|_{i \neq j} \xrightarrow{Z \rightarrow \infty} \text{Diagram} \quad (3.16)$$

From simple power counting follows the general rule, that when ever two vertices are connected by at least three propagators they must carry the same site index. The same arguments hold for the other diagrams in the skeleton expansion such that only local diagrams yield non-vanishing contributions and thus the self-energy becomes local for $Z \rightarrow \infty$. The self-energy contributions, however also include diagrams with different site indices as

can be seen from the following diagram:



$$\propto \left(\frac{1}{\sqrt{Z}} \right)^2. \quad (3.17)$$

It describes a process including electrons traveling from site i to j and returning after some time to site i . These retardation effects, also referred to as local quantum fluctuations, are the origin of the frequency dependence of the self-energy. The underlying skeleton diagram is, however, purely local. Now that we have convinced ourselves that the self-energy does not scale with Z , a look at Eq.(3.5) makes clear that the local dressed propagator scales in the same way as the bare propagator:

$$G_{ii}(i\omega_n) \equiv G(i\omega_n) \propto \frac{1}{\sqrt{Z}}, \quad (3.18)$$

which verifies our assumption in Eq.(3.3). We want to emphasize that in infinite dimensions the locality of the self-energy and neglecting momentum conservation are exact results and only become an approximation when applied to a finite dimensional problem. One might ask what if we include non-local interactions? It turns out that all their contributions, except the purely static Hartree term (first diagram in Eq.(3.11)) vanishes for $d \rightarrow \infty$ and only purely local interactions remain dynamical [13].

3.2 Self-Consistent Mapping onto Impurity Model

The central idea of a mean-field theory is to reduce a lattice problem to an effective single-site problem that needs to be solved self-consistently. A well known classical example is Weiss mean-field theory for Ising like models. In the same spirit we are here interested in solving quantum mechanical lattice models in dynamical mean-field theory. In the limit of infinite dimensions the diagrammatic of a lattice model becomes equivalent to that of an impurity model with the same on-site interaction. This key result, obtained by Georges and Kotliar [14], provides the basis for a mean-field description of lattice models.

Our starting point² in formulating this mean-field description is the effective single-site action of the lattice Hamiltonian:

$$S_{eff} = - \int_0^\beta d\tau \int_0^\beta d\tau' \psi^*(\tau) \left[\mathcal{G}^0(\tau - \tau') \right]^{-1} \psi(\tau') + \int_0^\beta d\tau H_{loc}^I(\tau). \quad (3.19)$$

In this context the terminus "effective" shall emphasize that the above action emulates the local dynamics of the lattice problem. The bare Green's function $\mathcal{G}^0(\tau - \tau')$ in S_{eff} is commonly referred to as effective Weiss field and we choose it such that it coincides with that of an impurity model:

$$\mathcal{G}^0(i\omega_n) = (i\omega_n - \mu - \Delta(i\omega_n))^{-1}, \quad (3.20)$$

with the hybridization function $\Delta(i\omega_n)$ given by:

$$\Delta(i\omega_n) = \sum_k V_k^* (i\omega_n - \tilde{\epsilon}_k)^{-1} V_k. \quad (3.21)$$

We give a detailed derivation for the above expression for the bare AIM Green's function in Appendix B.2. It is important to note that $\tilde{\epsilon}_k$ is a parameter of the effective Weiss field which must not be confused with the dispersion ϵ_k on the original lattice. The effective action of Eq.(3.19), which is written in terms of Grassmann variables ψ , is equivalent to the Hamiltonian formulation of the AIM given in Eq.(2.10). We want to stress that $\mathcal{G}^0(i\omega_n)$ is not equivalent to the non-interacting local Green's function of the lattice model, rather it can be interpreted as the amplitude for electron exchange with an "effective bath" representing the lattice. In that way $\mathcal{G}^0(i\omega_n)$ takes local quantum fluctuations into account and due to its frequency dependence (or equiv. τ -dependence) we can speak of a "dynamical" mean-field theory, although there are no spatial fluctuations. The bare Green's function and the interacting Green's function of the effective single-site problem are related via Dyson's equation:

$$[\mathcal{G}^0(i\omega_n)]^{-1} = [\mathcal{G}(i\omega_n)]^{-1} + \Sigma(i\omega_n). \quad (3.22)$$

In order to obtain a closed mean-field description we need to find the corresponding self-consistency equation. Therefore we first express the Green's function of the original lattice problem in momentum space:

$$G(k, i\omega_n) = \frac{1}{i\omega_n + \mu - \epsilon_k - \Sigma(i\omega_n)}, \quad (3.23)$$

²There exist several methods to derive S_{eff} rigorously starting from the action of the lattice model [15]. A particular readable derivation, using the so called cavity method, is given in [13].

where we have used the result from above that in $d \rightarrow \infty$ the self-energy is momentum independent. At this point we see that the lattice topology only enters through the dispersion relation ϵ_k of the non-interacting electrons. The local Green's function follows from Fourier transformation which becomes for local quantities a simple summation over k :

$$\begin{aligned} G(i\omega_n) &\equiv G_{ll}(i\omega_n) = \sum_k e^{-i(r_l-r_l)k} \frac{1}{i\omega_n + \mu - \epsilon_k - \Sigma(i\omega_n)} \\ &= \sum_k \frac{1}{i\omega_n + \mu - \epsilon_k - \Sigma(i\omega_n)}. \end{aligned} \quad (3.24)$$

Since we want the interacting Green's function $\mathcal{G}(i\omega_n)$ of the effective action such that the hopping between bath and impurity is equivalent to the local dynamic of the electrons on the lattice, we claim:

$$\mathcal{G}(i\omega_n) \equiv G(i\omega_n). \quad (3.25)$$

Now we are in the position to write down a self-consistency scheme for calculating the DMFT-Green's function of the lattice model, or equivalently, the local self-energy:

1. Make an initial guess for the self-energy (e.g. $\Sigma = 0$).
2. Use this self-energy to calculate the local lattice Green's function: $G(i\omega_n) = \sum_k \frac{1}{i\omega_n + \mu - \epsilon_k - \Sigma(i\omega_n)}$. This is the point where, via the dispersion relation ϵ_k , the lattice type comes into play.
3. Dyson's equation gives the effective Weiss field:

$$\mathcal{G}^0(i\omega_n) = \left(G(i\omega_n)^{-1} + \Sigma(i\omega_n) \right)^{-1}.$$
4. Get the solution $\mathcal{G}(i\omega_n)$ of the impurity model corresponding to $\mathcal{G}^0(i\omega_n)$ and with the same U as in the lattice model. This is the difficult part!
5. Use Dyson's equation to obtain a new self-energy:

$$\Sigma(i\omega_n) = \mathcal{G}_0(i\omega_n)^{-1} - \mathcal{G}(i\omega_n)^{-1}.$$
6. Iterate until convergence, i.e. until the difference between new and old self-energy satisfies a convergence criterion.

By rewriting Eq.(3.24) in the following way:

$$\begin{aligned} G(i\omega_n) &= \int_{-\infty}^{\infty} d\epsilon \sum_k \frac{\delta(\epsilon - \epsilon_k)}{i\omega_n + \mu - \epsilon - \Sigma(i\omega_n)} \\ &= \int_{-\infty}^{\infty} d\epsilon \frac{D(\epsilon)}{i\omega_n + \mu - \epsilon - \Sigma(i\omega_n)}, \end{aligned} \quad (3.26)$$

we can make the expression similar to that of a Hilbert transform which for an arbitrary density of states $D(\epsilon)$ reads:

$$\tilde{D}(\zeta) = \int_{-\infty}^{\infty} d\epsilon \frac{D(\epsilon)}{\zeta - \epsilon}. \quad (3.27)$$

For the reciprocal transformation we write:

$$R[\tilde{D}(\zeta)] = \zeta. \quad (3.28)$$

We are now able to express the self-energy of Eq.(3.23) in terms of the reciprocal Hilbert transformation of the local Green's function:

$$R[G(i\omega_n)] = i\omega_n + \mu - \Sigma(i\omega_n). \quad (3.29)$$

In that way we obtain the desired self-consistency condition which takes the form of a functional equation for \mathcal{G}_0 and G :

$$\mathcal{G}_0^{-1}(i\omega_n) = -i\omega_n - \mu + G^{-1}(i\omega_n) + R[G(i\omega_n)]. \quad (3.30)$$

The form of the reciprocal Hilbert transformation depends on the lattice type. For the ∞ -dimensional Bethe lattice there exists an analytical expression for R .

Bethe Lattice. In Figure 3.1 we show the Bethe lattice for various values of Z . For $Z \rightarrow \infty$ the Bethe lattice yields a semicircular density of states:

$$D(\epsilon) = \frac{\sqrt{4t^2 - \epsilon^2}}{2\pi t^2}, \quad |\epsilon| < 2t. \quad (3.31)$$

In this limit the reciprocal Hilbert transform reads:

$$R[G] = t^2 G + G^{-1} \quad (3.32)$$

and the self-consistency equation takes the simple form:

$$\mathcal{G}_0^{-1}(i\omega_n) = i\omega_n + \mu - t^2 G(i\omega_n), \quad (3.33)$$

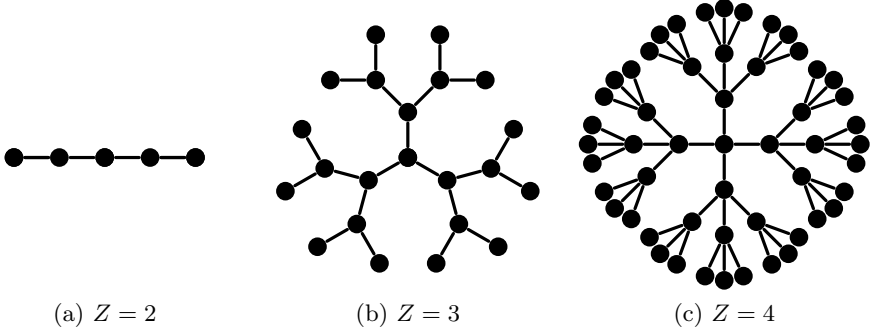


Figure 3.1: Bethe lattice for (a) $Z=2$, (b) $Z=3$ and (c) $Z=4$. For $Z = 2$ the Bethe lattice degenerates to a chain.

such that we do not need to perform the integral over the density of states. This lattice is primarily of theoretical interest because it results in a simplified self-consistency relation.

In the DMFT limit all the complexity in finding a solution to the lattice model is essentially reduced to finding a self-consistent solution of an impurity model. But solving the AIM is still a highly non-trivial task whose numerical expense crucially depends on the interaction type, the parameter regime, and the number of impurity orbitals taken into account.

Chapter 4

Continuous-Time Quantum Monte Carlo

Solving the AIM on the single- and two-particle level essentially amounts to the calculation of the corresponding single- and two-particle Green's functions. Green's functions can be derived from a partition function Z . The partition function is fundamental and thus the object of our central interest. Once we have a formal expression for Z , it will be straight forward to obtain the corresponding expression for the Green's functions.

The basic idea that all CTQMC methods have in common is to split the Hamiltonian of Eq.(2.10) into two parts:

$$H = H_a + H_b, \quad (4.1)$$

and to employ an interaction representation in which the imaginary time evolution of any operator \mathcal{O} is given by H_a :

$$\mathcal{O}(\tau) = e^{H_a\tau} \mathcal{O} e^{-H_a\tau}. \quad (4.2)$$

In this interaction representation the partition function can be expanded in terms of H_b which results in the following expression (for details see Appendix C):

$$\begin{aligned} Z = \text{Tr} \left[e^{-\beta H} \right] &= \text{Tr} \left[e^{-\beta H_a} T_\tau e^{-\int_0^\beta d\tau H_b(\tau)} \right] \\ &= \sum_{n=0}^{\infty} \int_0^\beta d\tau_1 \dots \int_0^\beta d\tau_n \frac{(-1)^n}{n!} \text{Tr} \left[T_\tau e^{-(\beta-\tau_1)H_a} H_b \dots e^{-(\tau_{n-1}-\tau_n)H_a} H_b e^{-\tau_n H_a} \right]. \end{aligned} \quad (4.3)$$

The above sum is then sampled simultaneously over all expansion orders n and all times $\{\tau_1, \dots, \tau_n\}$ in a Monte Carlo sampling procedure. Since the

factor $\frac{1}{n!}$ generically suppresses high expansion orders, there is no artificial truncation required. Further more, at no point a time discretization is introduced, so there is no discretization error as in the Hirsch-Fye algorithm [16].

In the context of impurity models four expansion types, differing primarily in the choice of H_b , have been formulated: CT-INT [17], CT-AUX [18], CT-J [19] and CT-HYB [20, 21]. A detailed discussion of each algorithm can be found in [22, 23]. In this thesis we exclusively concentrate on the hybridization expansion algorithm (CT-HYB) where the expansion is done in powers of the hybridization: $H_b = H_{hyb}$. One of the advantages of this algorithm is that complicated interactions, like Slater-Kanamori or a spherical-symmetric Coulomb interaction, can be treated as long as the local Hilbert space is not too large. In general $[H_{hyb}, H_{loc}] \neq 0$, such that at least one operator is not diagonal and the expansion generically requires the manipulation of matrices, whose size grow exponentially with the number of impurity orbitals. For general interactions H_{loc} , i.e. interactions that are not necessarily of density-density type, the computational bottleneck of the algorithm turns out to be the calculation of the local trace. This limits state of the art simulations to 5 spin degenerate bands with an Hilbert space size of $4^5 = 1024$ and makes the CT-HYB algorithm favorable for models with a moderate number of bands but with complicated interaction. It is best suited for single-site DMFT for materials with partially filled d and f shells, where the ability to treat complex multiplet interactions, like the Coulomb model, is necessary to describe the physics of the system accurately.

We start in the first section of this chapter with a detailed derivation of the hybridization expansion, i.e. the partition function expansion in CT-HYB. In the second section we explain how Monte Carlo sampling of this diagrammatic expansion works. In the last section we derive the formulas required to measure single- and two-particle Green's functions in the Monte Carlo procedure.

4.1 The Hybridization Expansion

In the hybridization expansion the impurity model Hamiltonian of Eq.(2.10) is split in the following way:

$$H_a = H_{bath} + H_{loc}, \quad H_b = H_{hyb}, \quad (4.4)$$

with the hybridization given by:

$$H_{hyb} = \underbrace{\sum_{k,\alpha} V_k^\alpha a_{k\alpha}^\dagger c_\alpha}_{\equiv \tilde{H}_{hyb}} + \underbrace{\sum_{k,\alpha} V_k^{\alpha*} c_\alpha^\dagger a_{k\alpha}}_{\equiv \tilde{H}_{hyb}^\dagger}. \quad (4.5)$$

It turns out to be favorable to expand simultaneously in \tilde{H}_{hyb} and \tilde{H}_{hyb}^\dagger and not directly in H_{hyb} . In that way we get immediately rid of the $(-1)^n$ factor. Since each term in the hybridization contains one creation and one annihilation operator, only even powers of the expansion with an equal number of alternately appearing \tilde{H}_{hyb} and \tilde{H}_{hyb}^\dagger operators contribute to a non-vanishing trace:

$$Z = \sum_{n=0}^{\infty} \int_0^\beta d\tau_1 \dots \int_0^\beta d\tau_n \int_0^\beta d\tau'_1 \dots \int_0^\beta d\tau'_n \frac{(-1)^{2n}}{(n!)^2} \quad (4.6)$$

$$\text{Tr} \left[T_\tau e^{-\beta H_a} \tilde{H}_{hyb}(\tau_1) \tilde{H}_{hyb}^\dagger(\tau'_1) \dots \tilde{H}_{hyb}(\tau_n) \tilde{H}_{hyb}^\dagger(\tau'_n) \right].$$

Substituting the explicit expressions for \tilde{H}_{hyb} and \tilde{H}_{hyb}^\dagger gives:

$$Z = \sum_{n=0}^{\infty} \int_0^\beta d\tau_1 \dots \int_0^\beta d\tau_n \int_0^\beta d\tau'_1 \dots \int_0^\beta d\tau'_n \frac{1}{(n!)^2} \quad (4.7)$$

$$\times \sum_{\substack{\alpha_1, \dots, \alpha_n \\ \alpha'_1, \dots, \alpha'_n}} \sum_{\substack{k_1, \dots, k_n \\ k'_1, \dots, k'_n}} V_{k_1}^{\alpha_1} V_{k'_1}^{\alpha'_1*} \dots V_{k_n}^{\alpha_n} V_{k'_n}^{\alpha'_n*}$$

$$\times \text{Tr} \left[T_\tau e^{-\beta H_a} a_{k_1 \alpha_1}^+(\tau_1) c_{\alpha_1}(\tau_1) c_{\alpha'_1}^+(\tau'_1) a_{k'_1 \alpha'_1}(\tau'_1) \dots \right.$$

$$\left. \times a_{k_n \alpha_n}^+(\tau_n) c_{\alpha_n}(\tau_n) c_{\alpha'_n}^+(\tau'_n) a_{k'_n \alpha'_n}(\tau'_n) \right].$$

We collect¹ bath and impurity operators in two separate traces:

$$\begin{aligned}
Z &= \sum_{n=0}^{\infty} \int_0^{\beta} d\tau_1 \dots \int_0^{\beta} d\tau_n \int_0^{\beta} d\tau'_1 \dots \int_0^{\beta} d\tau'_n \frac{1}{(n!)^2} \\
&\times \sum_{\substack{\alpha_1, \dots, \alpha_n \\ \alpha'_1, \dots, \alpha'_n}} \sum_{\substack{k_1, \dots, k_n \\ k'_1, \dots, k'_n}} V_{k_1}^{\alpha_1} V_{k'_1}^{\alpha'_1*} \dots V_{k_n}^{\alpha_n} V_{k'_n}^{\alpha'_n*} \\
&\times \text{Tr}_c \left[T_{\tau} e^{-\beta(H_{loc}^0 + H_{loc}^I)} c_{\alpha_1}(\tau_1) c_{\alpha'_1}^+(\tau'_1) \dots c_{\alpha_n}(\tau_n) c_{\alpha'_n}^+(\tau'_n) \right] \\
&\times \text{Tr}_a \left[T_{\tau} e^{-\beta H_{bath}} a_{k_1 \alpha_1}^+(\tau_1) a_{k'_1 \alpha'_1}(\tau'_1) \dots a_{k_n \alpha_n}^+(\tau_n) a_{k'_n \alpha'_n}(\tau'_n) \right].
\end{aligned} \tag{4.8}$$

The bath operators are non-interacting, we can therefore use the Wick theorem to obtain further simplifications. We demonstrate this at the following second-order term:

$$\sum_{\substack{k_1, k_2 \\ k'_1, k'_2}} V_{k_1}^{\alpha_1} V_{k'_1}^{\alpha'_1*} V_{k_2}^{\alpha_2} V_{k'_2}^{\alpha'_2*} \text{Tr}_a \left[T_{\tau} e^{-\beta H_{bath}} a_{k_1 \alpha_1}^+(\tau_1) a_{k'_1 \alpha'_1}(\tau'_1) a_{k_2 \alpha_2}^+(\tau_2) a_{k'_2 \alpha'_2}(\tau'_2) \right]. \tag{4.9}$$

Introducing the bath partition function

$$Z_{bath} = \text{Tr}_a [e^{-\beta H_{bath}}], \tag{4.10}$$

and the simplified notation for the thermal expectation value of the bath operators

$$\langle \dots \rangle_a = \frac{1}{Z_{bath}} \text{Tr}_a [T_{\tau} e^{-\beta H_{bath}} \dots], \tag{4.11}$$

we see that the second-order term of Eq.(4.9) can be contracted in the following way:

$$\begin{aligned}
&Z_{bath} \sum_{\substack{k_1, k_2 \\ k'_1, k'_2}} V_{k_1}^{\alpha_1} V_{k'_1}^{\alpha'_1*} V_{k_2}^{\alpha_2} V_{k'_2}^{\alpha'_2*} \langle \overbrace{a_{k_1 \alpha_1}^+(\tau_1) a_{k'_1 \alpha'_1}(\tau'_1)}^{+} \overbrace{a_{k_2 \alpha_2}^+(\tau_2) a_{k'_2 \alpha'_2}(\tau'_2)}^{+} \rangle_a \\
&= Z_{bath} \left(\sum_{k_1, k'_1} V_{k_1}^{\alpha_1} V_{k'_1}^{\alpha'_1*} \langle a_{k_1 \alpha_1}^+(\tau_1) a_{k'_1 \alpha'_1}(\tau'_1) \rangle_a \sum_{k_2, k'_2} V_{k_2}^{\alpha_2*} V_{k'_2}^{\alpha'_2*} \langle a_{k_2 \alpha_2}^+(\tau_2) a_{k'_2 \alpha'_2}(\tau'_2) \rangle_a - \right. \\
&\quad \left. - \sum_{k_1, k'_2} V_{k_1}^{\alpha_1} V_{k'_2}^{\alpha'_2*} \langle a_{k_1 \alpha_1}^+(\tau_1) a_{k'_2 \alpha'_2}(\tau'_2) \rangle_a \sum_{k'_1, k_2} V_{k'_1}^{\alpha'_1} V_{k_2}^{\alpha_2*} \langle a_{k'_1 \alpha'_1}^+(\tau'_1) a_{k_2 \alpha_2}(\tau_2) \rangle_a \right).
\end{aligned} \tag{4.12}$$

¹Since in this process each bath operator is anti-commuted with an even number of impurity operators the overall sign is unchanged.

Keeping in mind that there is still an ordering symbol T_τ in each $\langle \dots \rangle_a$ we can define the elements of the hybridization matrix Δ via:

$$\begin{aligned}
\Delta_{\alpha_i \alpha_j}(\tau_i, \tau_j) &\equiv \sum_{k_i, k_j} \delta_{k_i, k_j} V_{k_i}^{\alpha_i} V_{k_j}^{\alpha_j} \langle a_{k_i \alpha_i}^+(\tau_i) a_{k_j \alpha_j}(\tau_j) \rangle_a \\
&= \sum_k V_k^{\alpha_i} V_k^{\alpha_j} \langle a_{k \alpha_i}^+(\tau_i) a_{k \alpha_j}(\tau_j) \rangle_a \\
&= \sum_k V_k^{\alpha_i} V_k^{\alpha_j} \langle e^{\tau_i H_{bath}} a_{k \alpha_i}^\dagger e^{-(\tau_i - \tau_j) H_{bath}} a_{k \alpha_j} e^{-\tau_j H_{bath}} \rangle_a \\
&= \sum_k \frac{V_k^{\alpha_i} V_k^{\alpha_j}}{1 + e^{-\beta \epsilon_k}} \times \begin{cases} e^{-\epsilon_k(\tau_i - \tau_j)} & , 0 < (\tau_i - \tau_j) < \beta \\ -e^{-\epsilon_k(\beta - \tau_i + \tau_j)} & , -\beta < \tau_i - \tau_j < 0, \end{cases}
\end{aligned} \tag{4.13}$$

where we have used the fact that the expectation value is non-vanishing only for $k_i = k'_j \equiv k$. The second-order term can now be written as determinant of the hybridization matrix:

$$\det \Delta = \begin{vmatrix} \Delta_{\alpha_1 \alpha'_1}(\tau_1, \tau'_1) & \Delta_{\alpha_1 \alpha'_2}(\tau_1, \tau'_2) \\ \Delta_{\alpha_2 \alpha'_1}(\tau_2, \tau'_1) & \Delta_{\alpha_2 \alpha'_2}(\tau_2, \tau'_2) \end{vmatrix} \tag{4.14}$$

$$= \Delta_{\alpha_1 \alpha'_1}(\tau_1, \tau'_1) \Delta_{\alpha_2 \alpha'_2}(\tau_2, \tau'_2) - \Delta_{\alpha_1 \alpha'_2}(\tau_1, \tau'_2) \Delta_{\alpha_2 \alpha'_1}(\tau_2, \tau'_1)$$

This holds also for the higher-order terms, so that the partition function takes the form:

$$\begin{aligned}
Z = Z_{bath} \sum_{n=0}^{\infty} \int_0^\beta d\tau_1 \dots \int_0^\beta d\tau_n \int_0^\beta d\tau'_1 \dots \int_0^\beta d\tau'_n \frac{1}{(n!)^2} \sum_{\substack{\alpha_1 \dots \alpha_n \\ \alpha'_1 \dots \alpha'_n}} \\
\times \text{Tr}_c \left[T_\tau e^{-\beta H_{loc}} c_{\alpha_1}(\tau_1) c_{\alpha'_1}^+(\tau'_1) \dots c_{\alpha_n}(\tau_n) c_{\alpha'_n}^+(\tau'_n) \right] \det \Delta.
\end{aligned} \tag{4.15}$$

As discussed in Appendix C we can remove the factorials and change integration bounds due to the time ordering. This leads us to the following expression for the partition function expansion:

$$\begin{aligned}
Z = Z_{bath} \sum_{n=0}^{\infty} \int_0^\beta d\tau_1 \dots \int_{\tau_{n-1}}^\beta d\tau_n \int_0^\beta d\tau'_1 \dots \int_{\tau'_{n-1}}^\beta d\tau'_n \sum_{\substack{\alpha_1 \dots \alpha_n \\ \alpha'_1 \dots \alpha'_n}} \\
\times \text{Tr}_c \left[T_\tau e^{-\beta H_{loc}} c_{\alpha_1}(\tau_1) c_{\alpha'_1}^+(\tau'_1) \dots c_{\alpha_n}(\tau_n) c_{\alpha'_n}^+(\tau'_n) \right] \det \Delta.
\end{aligned} \tag{4.16}$$

If the bath is diagonal in the spin-band space, i.e.

$$\Delta_{\alpha_i \alpha_j}(\tau_i, \tau_j) = \delta_{\alpha_i \alpha_j} \Delta_{\alpha_i}(\tau_i, \tau_j), \tag{4.17}$$

the hybridization matrix Δ becomes block diagonal and its determinant becomes the product of determinants of smaller matrices Δ_i :

$$\det \Delta = \det \begin{pmatrix} \Delta_1 & & \\ & \ddots & \\ & & \Delta_k \end{pmatrix} = \prod_{i=1}^n \det \Delta_i. \quad (4.18)$$

Hence, the partition function expansion for a spin-band diagonal bath takes the form:

$$\begin{aligned} Z = & Z_{bath} \sum_{n=0}^{\infty} \int_0^{\beta} d\tau_1 \dots \int_{\tau_{n-1}}^{\beta} d\tau_n \int_0^{\beta} d\tau'_1 \dots \int_{\tau'_{n-1}}^{\beta} d\tau'_n \sum_{\alpha_1 \dots \alpha_n} \\ & \times \text{Tr}_c \left[T_{\tau} e^{-\beta H_{loc}} c_{\alpha_1}(\tau_1) c_{\alpha_1}^+(\tau'_1) \dots c_{\alpha_n}(\tau_n) c_{\alpha_n}^+(\tau'_n) \right] \prod_{i=1}^n \det \Delta_i. \end{aligned} \quad (4.19)$$

4.2 Monte Carlo Sampling of the Partition Function

The expression Eq.(4.16) for the partition function may be interpreted as an integral over all the configurations x of weight $dx w(x)$ in the configuration space \mathcal{C} :

$$Z = \int_{\mathcal{C}} dx w(x). \quad (4.20)$$

According to Eq.(4.16) a configuration $x = (n, \alpha, \tau) \in \mathcal{C}$ is characterized by the expansion order n , the combined spin-band indices α and the different imaginary time arguments τ . Each configuration can then be visualized as a graph of a diagrammatic expansion. The weight of a possible second-order configuration amounts to:

$$\begin{aligned} w = & Z_{bath} \text{Tr}_c \left[T_{\tau} e^{-\beta H_{loc}} c_{\uparrow}(\tau_1) c_{\uparrow}^+(\tau'_1) c_{\uparrow}(\tau_2) c_{\uparrow}^+(\tau'_2) \right] \\ & \times (\Delta_{\uparrow}(\tau_1, \tau'_1) \Delta_{\uparrow}(\tau_2, \tau'_2) - \Delta_{\uparrow}(\tau_1, \tau'_2) \Delta_{\uparrow}(\tau_2, \tau'_1)). \end{aligned} \quad (4.21)$$

In the above example all the operators have the same spin index so we get both contributions from the hybridization determinant Eq.(4.14). Another second-order example, where we have operators with different spin index, reads:

$$w = Z_{bath} \text{Tr}_c \left[T_{\tau} e^{-\beta H_{loc}} c_{\uparrow}(\tau_1) c_{\downarrow}^+(\tau'_1) c_{\downarrow}(\tau_2) c_{\uparrow}^+(\tau'_2) \right] \times (-\Delta_{\uparrow}(\tau_1, \tau'_2) \Delta_{\downarrow}(\tau_2, \tau'_1)). \quad (4.22)$$

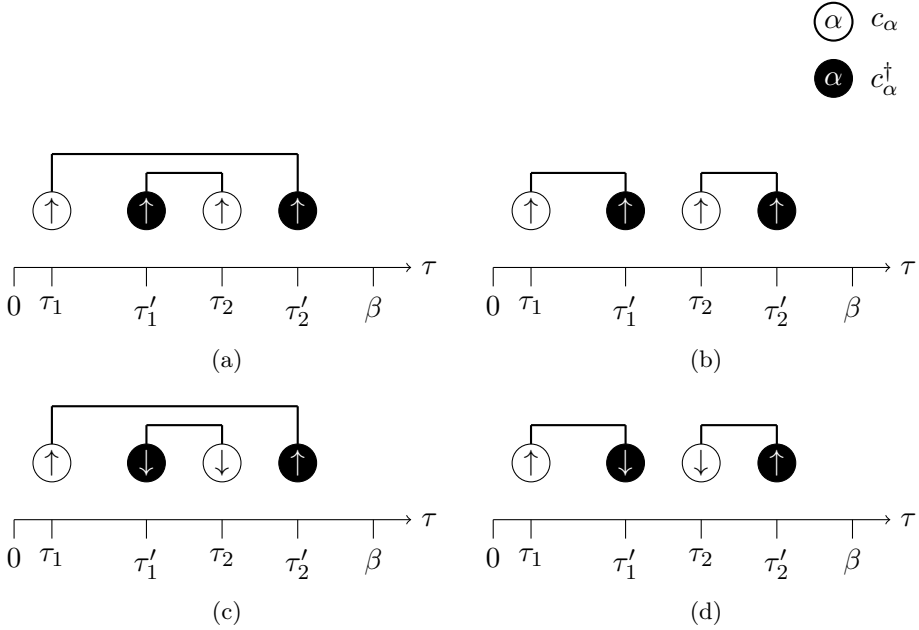


Figure 4.1: Possible second-order configurations of a single-band model ($\alpha = \uparrow, \downarrow$). The circles correspond to the impurity operators and the fat solid bars to hybridization functions. Configurations (a) and (b) with all spins up contribute to the weight given in Eq.(4.21). In the spin diagonal case only configuration (c) contributes to the weight of Eq.(4.22). Configuration (d) is killed by the Kronecker delta in Eq.(4.17).

Here we get, due to the Kronecker delta in Eq.(4.17), only one contribution from the determinant. Diagrammatic representations of these specific configurations are shown in Figure 4.1.

Expectation values of observables are given by the weighted average over the configuration space:

$$\langle A \rangle_w = \frac{1}{Z} \int_{\mathcal{C}} dx A(x) w(x). \quad (4.23)$$

This expectation value can be approximated in a Monte Carlo importance sampling procedure:

$$\langle A \rangle_w \stackrel{MC}{\approx} \langle A \rangle_{MC} = \frac{1}{N} \sum_{i=1}^N A(x_i), \quad (4.24)$$

where the N random configurations x_i are chosen such that they follow the probability distribution:

$$p(x) = \frac{w(x)}{Z}. \quad (4.25)$$

According to the central limit theorem, the Monte Carlo average of Eq.(4.24) is normally distributed around $\langle A \rangle_w$ and becomes exact in the limit of $N \rightarrow \infty$.

Markov Process. In order to generate configurations x_i which follow the probability distribution Eq.(4.25), as required in the MC-average of Eq.(4.24), we employ a Markov process. A Markov process is fully characterized by the transition probabilities W_{xy} to go, in a single step, from a configuration x to another configuration y . Starting from an arbitrary configuration, such a process converges after a finite number of steps to a stationary distribution $p(x)$ if it is ergodic² and if it fulfills the detailed balance condition:

$$\frac{W_{xy}}{W_{yx}} = \frac{w(y)}{w(x)}. \quad (4.26)$$

It is important to sample the configuration space according to the stationary distribution, since we are ultimately interested in evaluating expectation values of observables that correspond to the stationary state of the system under consideration.

Metropolis Algorithm. A well known algorithm which satisfies the detailed balance condition of Eq.(4.26) is the Metropolis algorithm. Therein the transition probability is split in the following way:

$$W_{xy} = W_{xy}^{prop} W_{xy}^{acc}, \quad (4.27)$$

so that the update from a given configuration x to another configuration y is proposed with the probability W_{xy}^{prop} , but only accepted with the probability W_{xy}^{acc} . The acceptance probability W_{xy}^{acc} is given by:

$$W_{xy}^{acc} = \min[1, R_{xy}], \quad (4.28)$$

where the acceptance ratio R_{xy} reads:

$$R_{xy} = \frac{w(y)W_{yx}^{prop}}{w(x)W_{xy}^{prop}}. \quad (4.29)$$

If the proposed configuration y is rejected, the old configuration x is used again.

²Each configuration in \mathcal{C} must be reachable from each other configuration in \mathcal{C} in a finite number of steps.

Sampling the Partition Function. Standard updates, which fulfill the ergodicity condition, consist in adding/removing a creator-annihilator pair. Due to the double Taylor expansion a term of order n has $2n$ operators, so these updates increase/decrease the expansion order by one. In the following we label configurations with their expansion order n , such that the partition function takes the following form:

$$Z = \sum \int \underbrace{\left(\prod_{i=1}^n d\tau_i d\tau'_i \right)}_{p(n)} w(n), \quad (4.30)$$

with $w(n)$ given by:

$$w(n) = Z_{bath} \text{Tr}_c \left[T_\tau e^{-\beta H_{loc}} c_{\alpha_1}(\tau_1) c_{\alpha'_1}^+(\tau'_1) \dots c_{\alpha_n}(\tau_n) c_{\alpha'_n}^+(\tau'_n) \right] \det \Delta. \quad (4.31)$$

The proposal probability of inserting a operator pair with time labels τ_i and τ'_i amounts to:

$$W_{n,n+1}^{prop} = \frac{d\tau_i d\tau'_i}{\beta^2}. \quad (4.32)$$

The removal probability of a randomly chosen pair out of $(n+1)^2$ existing pairs reads:

$$W_{n+1,n}^{prop} = \frac{1}{(n+1)^2}. \quad (4.33)$$

The acceptance ratio becomes:

$$\begin{aligned} R_{n,n+1} &= \frac{p(n+1) W_{n+1,n}^{prop}}{p(n) W_{n,n+1}^{prop}} \\ &= \frac{\left(\prod_{i=1}^n d\tau_i d\tau'_i \right) d\tau_j d\tau'_j w(n+1) \frac{1}{(n+1)^2}}{\left(\prod_{i=1}^n d\tau_i d\tau'_i \right) w(n) \frac{d\tau_j d\tau'_j}{\beta^2}} \\ &= \frac{w(n+1)}{w(n)} \frac{\beta^2}{(n+1)^2}. \end{aligned} \quad (4.34)$$

Substituting Eq.(4.31) gives:

$$R_{n,n+1} = \frac{\text{Tr}_c \left[T_\tau e^{-\beta H_{loc}} c_{\alpha_1}(\tau_1) c_{\alpha'_1}^+(\tau'_1) \dots c_{\alpha_{n+1}}(\tau_{n+1}) c_{\alpha'_{n+1}}^+(\tau'_{n+1}) \right] \det \Delta'}{\text{Tr}_c \left[T_\tau e^{-\beta H_{loc}} c_{\alpha_1}(\tau_1) c_{\alpha'_1}^+(\tau'_1) \dots c_{\alpha_n}(\tau_n) c_{\alpha'_n}^+(\tau'_n) \right] \det \Delta} \frac{\beta^2}{(n+1)^2}. \quad (4.35)$$

For the spin-band diagonal bath (see Eq.(4.19)) the above expression simplifies:

$$R_{n,n+1} = \frac{\text{Tr}_c \left[T_\tau e^{-\beta H_{loc}} c_{\alpha_1}(\tau_1) c_{\alpha_1}^+(\tau'_1) \dots c_{\alpha_{n+1}}(\tau_{n+1}) c_{\alpha_{n+1}}^+(\tau'_{n+1}) \right] \det \Delta_{n+1}}{\text{Tr}_c \left[T_\tau e^{-\beta H_{loc}} c_{\alpha_1}(\tau_1) c_{\alpha_1}^+(\tau'_1) \dots c_{\alpha_n}(\tau_n) c_{\alpha_n}^+(\tau'_n) \right]} \frac{\beta^2}{(n+1)^2}. \quad (4.36)$$

The acceptance ratio for the inverse process (removing an operator pair) is given by:

$$R_{n+1,n} = R_{n,n+1}^{-1}. \quad (4.37)$$

For a spin-band diagonal bath the computation of the hybridization determinant is computationally inexpensive (see Eq.(4.14)). If only density-density interactions are taken into account, the local Hamiltonian is diagonal in the occupation number representation. In this case there exists an efficient procedure, the segment algorithm [22], to evaluate the acceptance ratio of Eq.(4.36). For more general interactions, where the local Hamiltonian is not diagonal, the calculation of the local trace in Eq.(4.36) is a delicate task and the computational bottleneck of the algorithm. A straight forward approach [21] consists in representing the creation and annihilation operators in the eigenbasis of the local Hamiltonian, which has the advantage that the propagator $e^{-\beta H_{loc}}$ is diagonal. If the local Hamiltonian has symmetries, it is favorable to transform it to a basis where it takes a block diagonal form to reduce the computational effort in calculating the matrix-matrix products [24]. An alternative approach, the Krylov implementation, has been proposed by Läuchli and Werner [25]. They stay in the occupation number basis where the Hamiltonian and the hybridization operators are sparse and use efficient Krylov-space algorithms to calculate the matrix exponential required for the imaginary time evolution.

4.3 Measuring Correlation Functions

In order to derive the Monte Carlo accumulation formulas for the single- and two-particle Green's function it is favorable to represent the partition function as path integral over Grassmann variables:

$$Z = e^{-E[\Delta]} = \int \mathcal{D}c^+ \mathcal{D}c e^{-S}. \quad (4.38)$$

The action of the impurity model is given by:

$$S = - \int_0^\beta d\tau \int_0^\beta d\tau' \sum_\alpha c_\alpha^+(\tau) \left[\mathcal{G}_\alpha^0(\tau - \tau') \right]^{-1} c_\alpha(\tau') + \int_0^\beta d\tau H_{loc}^I(\tau), \quad (4.39)$$

where the bare Green's function reads:

$$\mathcal{G}_\alpha^0(i\omega_n) = (i\omega_n - \mu - \Delta_\alpha(i\omega_n))^{-1}. \quad (4.40)$$

Above we have introduced the functional:

$$E[\Delta] = -\ln Z[\Delta], \quad (4.41)$$

which we will use as generating functional for connected correlation functions. Furthermore we introduce functional derivatives in the following way:

$$\frac{\delta}{\delta \Delta_\beta(\tau_c, \tau_d)} \Delta_\alpha(\tau_a, \tau_b) = \delta_{\alpha\beta} \delta(\tau_a - \tau_c) \delta(\tau_b - \tau_d). \quad (4.42)$$

In the above formulas we have implicitly assumed that our hybridization matrix and the interaction matrix is block diagonal in the spin-band space, which in turn results in single-particle Green's function with only one combined index. For the case of non-diagonal interaction the hybridization must also include off-diagonal contributions in order to serve as a source term in the partition function. The single-particle Green's function then comes with two combined indices.

Single-Particle Green's Function. Now we are in the position to obtain correlation functions from the generating functional $E[\Delta]$ via functional derivatives w.r.t. hybridization functions:

$$\begin{aligned} \frac{\delta E}{\delta \Delta_\alpha(\tau_2, \tau_1)} &= -\frac{1}{Z} \frac{\delta Z}{\delta \Delta_\alpha(\tau_2, \tau_1)} \\ &= \frac{1}{Z} \int \mathcal{D}c^+ \mathcal{D}c c_\alpha^+(\tau_2) c_\alpha(\tau_1) e^{-S} \\ &= \langle T_\tau c_\alpha^+(\tau_2) c_\alpha(\tau_1) \rangle = -\langle T_\tau c_\alpha(\tau_1) c_\alpha^+(\tau_2) \rangle. \end{aligned} \quad (4.43)$$

From the definition of the single-particle Green's function Eq.(2.23) we immediately see that:

$$\frac{\delta E}{\delta \Delta_\alpha(\tau_2, \tau_1)} = G_\alpha(\tau_1, \tau_2). \quad (4.44)$$

In order to obtain the formula for the Monte Carlo weights, we must use the explicit expression for the partition function Eq.(4.19), which we repeat here for convenience:

$$\begin{aligned} Z = Z_{bath} &\sum_{n=0}^{\infty} \int_0^\beta d\tau_1 \dots \int_{\tau_{n-1}}^\beta d\tau_n \int_0^\beta d\tau'_1 \dots \int_{\tau'_{n-1}}^\beta d\tau'_n \sum_{\alpha_1 \dots \alpha_n} \\ &\times \text{Tr}_c \left[T_\tau e^{-\beta H_{loc}} c_{\alpha_1}(\tau_1) c_{\alpha_1}^+(\tau'_1) \dots c_{\alpha_n}(\tau_n) c_{\alpha_n}^+(\tau'_n) \right] \det \Delta. \end{aligned} \quad (4.45)$$

The generating functional takes the form:

$$E[\Delta] = -\ln Z_{bath} \sum \int \text{Tr}_c[\dots] \det \Delta. \quad (4.46)$$

To get the corresponding expression for the Green's function we need to take the derivative from the determinant part only, since the local trace $\text{Tr}_c[\dots]$ contains no hybridization functions:

$$G_\alpha(\tau_1, \tau_2) = -\frac{1}{Z_{bath} \sum \int \text{Tr}_c[\dots] \det \Delta} Z_{bath} \sum \int \text{Tr}_c[\dots] \frac{\delta \det \Delta}{\delta \Delta_\alpha(\tau_2, \tau_1)}. \quad (4.47)$$

We use Jacobi's formula to get the derivative of the determinant w.r.t. a matrix element A_{ab} :

$$\frac{\partial}{\partial A_{ab}} \det A = \det A (A^{-1})_{ba}. \quad (4.48)$$

Using the above identity for the hybridization determinant and introducing $M_\alpha(\tau_i, \tau_j) \equiv \Delta_\alpha^{-1}(\tau_i, \tau_j)$ we get:

$$\frac{\delta \det \Delta}{\delta \Delta_\alpha(\tau_2, \tau_1)} = \det \Delta \times M_\alpha(\tau_1, \tau_2). \quad (4.49)$$

The Green's function can now be written as:

$$G_\alpha(\tau_1, \tau_2) = -\frac{1}{Z} Z_{bath} \sum \int \text{Tr}_c[\dots] \det \Delta M_\alpha(\tau_1, \tau_2). \quad (4.50)$$

Comparing the last expression to Eq.(4.23) and Eq.(4.24) allows us to identify the estimators for the Green's function, i.e. the quantities that are averaged in the MC procedure:

$$G_\alpha(\tau_1, \tau_2) \stackrel{MC}{\approx} -\langle M_\alpha(\tau_1, \tau_2) \rangle_{MC} = -\frac{1}{N} \sum_{\mathcal{C}} M_\alpha(\tau_1, \tau_2). \quad (4.51)$$

The N random configurations $\{x\} \subset \mathcal{C}$ in the Monte Carlo average are generated according to the distribution:

$$p(x) = \frac{Z_{Bath} \det \Delta}{Z}, \quad (4.52)$$

using the Metropolis algorithm described in the previous section.

Two-Particle Green's Function. Though, a little more elaborate, the procedure for the two-particle correlation function works completely analogous to the single-particle case. Here we need to pull down four operators from the exponential, therefore we take two functional derivatives:

$$\begin{aligned}
\frac{\delta^2 E}{\delta \Delta_\alpha(\tau_2, \tau_1) \delta \Delta_\beta(\tau_4, \tau_3)} &= -\frac{1}{Z} \frac{\delta^2 Z}{\delta \Delta_\alpha(\tau_2, \tau_1) \delta \Delta_\beta(\tau_4, \tau_3)} + \\
&\quad + \frac{1}{Z^2} \frac{\delta Z}{\delta \Delta_\alpha(\tau_2, \tau_1)} \frac{\delta Z}{\delta \Delta_\beta(\tau_4, \tau_3)} \\
&= \langle T_\tau c_\alpha^+(\tau_2) c_\alpha(\tau_1) c_\beta^+(\tau_4) c_\beta(\tau_3) \rangle \\
&\quad - \langle T_\tau c_\alpha^+(\tau_2) c_\alpha(\tau_1) \rangle \langle T_\tau c_\beta^+(\tau_4) c_\beta(\tau_3) \rangle \\
&= \langle T_\tau c_\alpha(\tau_1) c_\alpha^+(\tau_2) c_\beta(\tau_3) c_\beta^+(\tau_4) \rangle \\
&\quad - \langle T_\tau c_\alpha(\tau_1) c_\alpha^+(\tau_2) \rangle \langle T_\tau c_\beta(\tau_3) c_\beta^+(\tau_4) \rangle \\
&\equiv \langle T_\tau c_\alpha(\tau_1) c_\alpha^+(\tau_2) c_\beta(\tau_3) c_\beta^+(\tau_4) \rangle_{\text{conn}}.
\end{aligned} \tag{4.53}$$

In the last line we have defined the connected part of the two-particle Green's function. By making the identification:

$$\frac{\delta^2 E}{\delta \Delta_\alpha(\tau_2, \tau_1) \delta \Delta_\beta(\tau_4, \tau_3)} = \chi_{\alpha\beta}(\tau_1, \tau_2, \tau_3, \tau_4), \tag{4.54}$$

we obtain the definition of the generalized susceptibility from Eq.(2.42):

$$\chi_{\alpha\beta}(\tau_1, \tau_2, \tau_3, \tau_4) = G_{\alpha\beta}(\tau_1, \tau_2, \tau_3, \tau_4) - G_\alpha(\tau_1, \tau_2) G_\beta(\tau_3, \tau_4). \tag{4.55}$$

Since the unconnected part can be completely expressed in terms of single-particle Green's functions, we only have to take care of the part where two derivatives act on the partition function:

$$\begin{aligned}
G_{\alpha\beta}(\tau_1, \tau_2, \tau_3, \tau_4) &= -\frac{1}{Z} \frac{\delta^2 Z}{\delta \Delta_\alpha(\tau_2, \tau_1) \delta \Delta_\beta(\tau_4, \tau_3)} \\
&= -\frac{1}{Z} Z_{\text{bath}} \sum \int \text{Tr}_c[\dots] \frac{\delta^2 \det \Delta}{\delta \Delta_\alpha(\tau_2, \tau_1) \delta \Delta_\beta(\tau_4, \tau_3)}.
\end{aligned} \tag{4.56}$$

To get the corresponding accumulation formula we need the second derivative of the hybridization determinant. Recursive application of Jacobi's formula Eq.(4.48) results, as demonstrated in Appendix D, in the following expression for the second derivative of a determinant:

$$\frac{\partial^2}{\partial A_{ab} \partial A_{cd}} \det A = \det A \left[(A^{-1})_{ba} (A^{-1})_{dc} - (A^{-1})_{da} (A^{-1})_{bc} \right]. \tag{4.57}$$

Applying the above expression to the hybridization determinant gives:

$$\frac{\delta^2 \det \Delta}{\delta \Delta_\alpha(\tau_2, \tau_1) \delta \Delta_\beta(\tau_4, \tau_3)} = \det \Delta \times [M_\alpha(\tau_1, \tau_2) M_\beta(\tau_3, \tau_4) - \delta_{\alpha, \beta} M_\alpha(\tau_1, \tau_4) M_\alpha(\tau_3, \tau_2)]. \quad (4.58)$$

The two-particle Green's function now reads:

$$G_{\alpha\beta}(\tau_1, \tau_2, \tau_3, \tau_4) = -\frac{1}{Z} Z_{bath} \sum \int \text{Tr}_c[\dots] \det \Delta \times [M_\alpha(\tau_1, \tau_2) M_\beta(\tau_3, \tau_4) - \delta_{\alpha, \beta} M_\alpha(\tau_1, \tau_4) M_\alpha(\tau_3, \tau_2)]. \quad (4.59)$$

We can now, in complete analogy to the single-particle case, identify the estimators for the two-particle Green's function:

$$G_{\alpha\beta}(\tau_1, \tau_2, \tau_3, \tau_4) \stackrel{MC}{\approx} \langle M_\alpha(\tau_1, \tau_2) M_\beta(\tau_3, \tau_4) - M_\alpha(\tau_1, \tau_2) M_\beta(\tau_3, \tau_4) \rangle_{MC} = \frac{1}{N} \sum_c (M_\alpha(\tau_1, \tau_2) M_\beta(\tau_3, \tau_4) - \delta_{\alpha, \beta} M_\alpha(\tau_1, \tau_4) M_\alpha(\tau_3, \tau_2)). \quad (4.60)$$

Chapter 5

Numerical Simulations

The main objective of this work was to implement and test a measurement routine for the two-particle Green's function in a CTQMC code. In this Chapter we present some of the results from our numerical simulations done with this code. As discussed in Chapter 2 the two-particle quantities we are interested in come with two spin and three τ -indices and in the multi-band case with two additional band indices. Because of the many indices these quantities are numerically costly to measure and result in rather huge data volumes. We restricted our simulations to the half-filled single-band case where the numerical effort which is necessary to provide proper statistics was manageable with the parallel performance of 12 CPU's within less than a week of runtime per simulation. Furthermore we had for comparison purposes an ED and a HF code to our disposal which are essentially both restricted to the single-band case. In each simulation 10 DMFT iterations were performed, which means our results represent DMFT solutions of the half-filled Hubbard model given in Eq.(2.8). In the first section of this chapter we compare the two-particle Green's function in τ -space from our CTQMC code to that from the HF algorithm. In the second section we compare the generalized susceptibilities in ω -space from CTQMC, HF and ED. We discuss in the third section how the numerical effort of our implementation scales with β and U . Finally, in the last section we document our approach of calculating the local spin susceptibility in the vicinity of the Mott-transition with our CTQMC code.

5.1 Two-Particle Quantities in τ -space

In order to check if our measurement routine works correctly we want to compare the two-particle results from our CTQMC code to the correspond-

ing results from the HF algorithm. In this comparison we take a look at the generalized susceptibilities with two of the three τ -indices fixed. As discussed in Appendix E in the Hirsch-Fye method the interval $[0, \beta)$ is split into N equally spaced slices. For $\beta = 10$ and $N = 100$ this means the Green's function is evaluated and stored at $\tau = 0, 0.1, 0.2, \dots, 9.9$. In the CTQMC code the Green's function is measured at randomly chosen τ -points out of the interval $[0, \beta)$. In the Monte Carlo routine these measurements are averaged in N_{bin} sub-intervals of $[0, \beta)$ and stored. These sub-intervals are called bins and the process of averaging therein is referred to as binning. For $\beta = 10$ and $N_{bin} = 50$, i.e., 50 bins of equal size, this results in the following partitioning: $[0, 10) = \{[0, 0.2), [0.2, 0.4), \dots, [9.8, 10.0)\}$. Due to the averaging in each bin the Green's function is evaluated at $\tau = 0.1, 0.3, \dots, 9.9$. That means when we choose $N_{bin} = 50$ in the CTQMC algorithm and $N = 100$ in the HF algorithm each point from CTQMC should be the average of every second point from the HF algorithm. In Figure 5.1 we compare the generalized susceptibilities $\chi_{\sigma\sigma'}$ in the DMFT limit on the Bethe lattice from the HF and the CTQMC method using the following Hubbard parameters: $U = 1.5$, $\beta = 10$, $\mu = U/2$. In the CTQMC method $\chi_{\sigma\sigma'}$ is built by subtracting the disconnected part $D_{\sigma\sigma'}$ (see Eq.(2.39)) from the full two-particle Green's function $G_{\sigma\sigma'}^{(2)}$. The later is the only quantity that is measured on the two-particle level, i.e., that is numerically costly. The disconnected part is built from single-particle Green's functions measured on the single-particle level. From Figure 5.1 we see that the susceptibilities from CT and HF lie practically on top. The only noteworthy differences appear at those values where the two-particle Green's function has a discontinuity, i.e., where $\tau_i = \tau_j$. This discrepancy is a result of the incorrect implementation of the Monte Carlo measurement at these special points. The following example should make this issue clear. Let us take a look at Figure 5.1c and therein at the discontinuity of the two-particle Green's function at $\tau_2 = \tau_3 = 3.7$. At this value the susceptibilities from HF and CTQMC differ clearly. Naively evaluating the two-particle Green's function at $\tau_3 = 3.7$ would amount to averaging the measurements in bin $(3.6, 3.8]$. But the measurements where $3.6 < \tau_3 < 3.7$ have positive and those where $3.7 < \tau_3 < 3.8$ have negative amplitude and averaging of these values clearly gives the wrong result. So how to proceed? We addressed this problem by discarding all measurements where $3.6 < \tau_3 < 3.7$ and multiplied the values of those where $3.7 < \tau_3 < 3.8$ with a factor of two. In that way we avoid at least the averaging across the discontinuity. However, by averaging in the interval $(3.7, 3.8]$ we assign to the point at $\tau_3 = 3.7$ the value that actually belongs to $\tau_3 = 3.75$. This

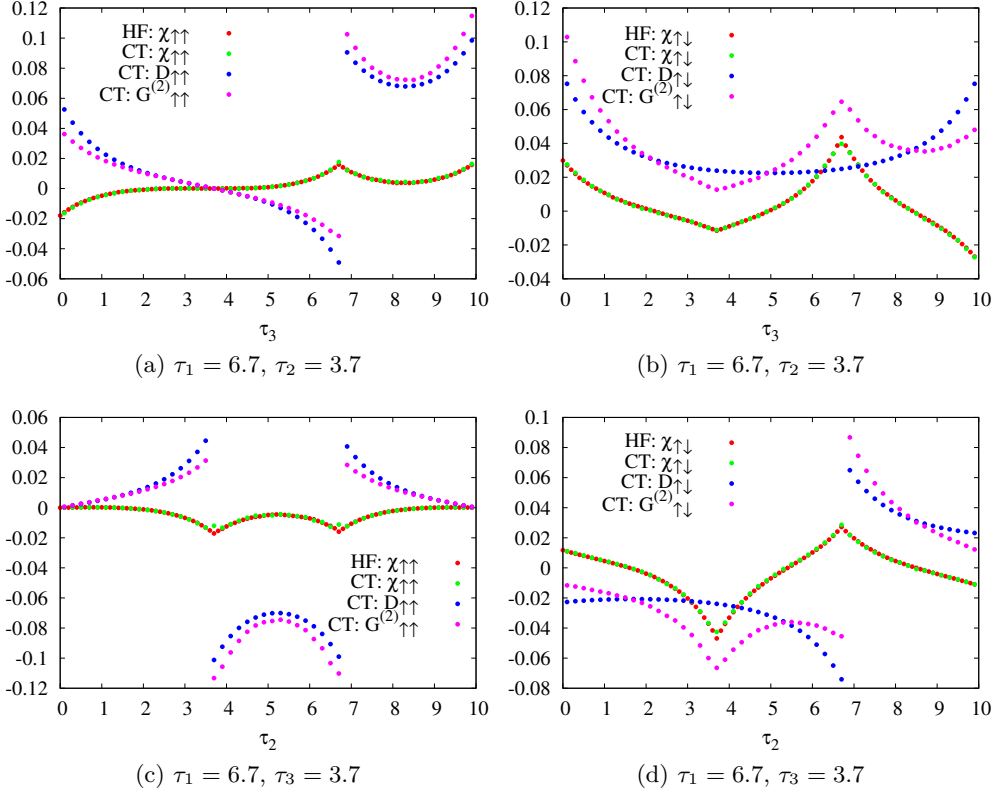


Figure 5.1: Comparison between the susceptibilities $\chi_{\sigma\sigma'}$ from the Continuous-Time (CT) and the Hirsch-Fye (HF) algorithm. Further, the disconnected part $D_{\sigma\sigma'}$ and the full two-particle Green's function $G_{\sigma\sigma'}^{(2)}$ from the CT algorithm are shown.

wrong assignment is reflected in the remaining discrepancies in Figure 5.1. The single-particle Green's function does not suffer from this problem and in turn the disconnected part from the two-particle Green's function, too. This can be directly seen from the definition of the single-particle Green's function:

$$G_{\sigma}(\tau = 0) = \langle T_{\tau} c_{\sigma}(0) c_{\sigma}^{\dagger} \rangle =: n_{\sigma}, \quad (5.1)$$

which is discontinuous only at $\tau = 0$. However, $G_{\sigma}(0)$ is per definition equivalent to the occupation number n_{σ} which can be simply calculated by counting the number of electrons that are added/removed during the update procedure. A direct generalization to the two-particle Green's function

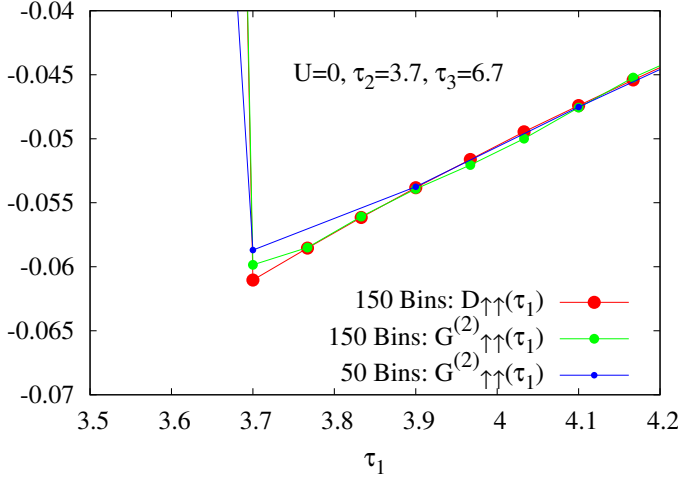


Figure 5.2: Study of the systematic (binning) error at the discontinuity. For $U=0$, the disconnected part $D_{\sigma\sigma'}$ and the full two-particle Green's function $G_{\sigma\sigma'}^{(2)}$ should be equivalent.

is not possible. We see this from the following inequality:

$$\begin{aligned}
 G_{\sigma\sigma'}(\tau, \tau, \tau_3) &= \langle T_\tau c_\sigma(\tau) c_\sigma^\dagger(\tau) c_{\sigma'}(\tau_3) c_{\sigma'} \rangle \\
 &= \langle T_\tau n_\sigma(\tau) c_{\sigma'}(\tau_3) c_{\sigma'} \rangle \\
 &\neq \langle T_\tau n_\sigma(\tau) \rangle \langle T_\tau c_{\sigma'}(\tau_3) c_{\sigma'} \rangle \\
 &= n_\sigma G_{\sigma'}(\tau_3).
 \end{aligned} \tag{5.2}$$

Since the number operator appears in company with the remaining two impurity operators the resulting thermal expectation value can not be evaluated by simple electron counting. We avoid to measure directly quantities like those of Eq.(5.2) by approximating them with the method discussed above. To study the influence of the bin-size on this error, we compare the disconnected part to the full two-particle Green's function for $U = 0$, where both should be equivalent. This comparison, for 50 and 150 bins, is shown in Figure 5.2. The result is with increasing N_{bin} the error is getting smaller.

5.2 Generalized Susceptibilities in Frequency-space

In our CTQMC code the two-particle Green's function is measured in τ -space. As discussed in Chapter 2 the transformation to frequency representation may be defined in various ways. We concentrate in this section

on the particle-hole representation given in Eq.(2.44). The spin and charge susceptibilities are defined as the following linear combinations of particle-hole susceptibilities:

$$\chi_d^{\nu\nu'\omega} := \chi_{ph,\uparrow\uparrow}^{\nu\nu'\omega} + \chi_{ph,\uparrow\downarrow}^{\nu\nu'\omega}, \quad (5.3)$$

$$\chi_m^{\nu\nu'\omega} := \chi_{ph,\uparrow\uparrow}^{\nu\nu'\omega} - \chi_{ph,\uparrow\downarrow}^{\nu\nu'\omega}. \quad (5.4)$$

In Figure 5.3 we compare the results from the Continuous-Time, Hirsch-

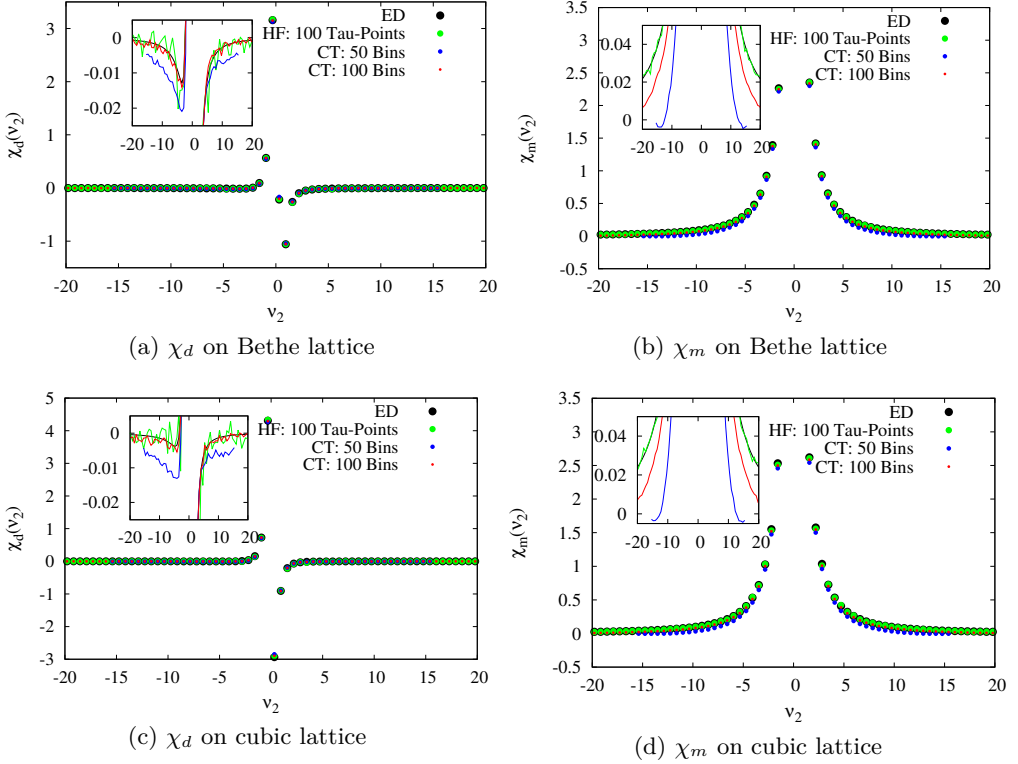


Figure 5.3: Comparison between charge (spin) susceptibility χ_d (χ_m) from CTQMC, HF and ED on Bethe and simple-cubic lattice. Systematic deviations can be seen in the enlarged views shown in the inlays.

Fye and Exact-Diagonalization method. We show the charge (spin) susceptibility χ_d (χ_m) in the DMFT limit on the Bethe and the simple cubic lattice. The plots are made with fixed values for $\omega = 0$ and $\nu_1 = 0.314$ (first Matsubara frequency). From the CT solver results are shown for 50 and 100 bins. The corresponding Hubbard parameters are: $U = 1.5$, $\beta = 10$, $\mu = U/2$. In the small inlays enlarged views are shown. These make a

systematic offset between the CTQMC results and those from HF and ED visible. This offset is correlated to the number of bins used in the CTQMC solver. We observe that this failure is smaller for 100 bins than in the calculation with 50 bins. We suspect that this systematic error originates in the assignment error at the discontinuity that we discussed in the previous section.

5.3 Performance Benchmark

In the hybridization algorithm the expansion order is distributed around some average value that is correlated to the parameters U and β of the Hubbard model (for details see [26]). During the sampling procedure the current configuration, and thus the expansion order, is changed by adding and removing creation and annihilation operators at randomly chosen τ -points in the local trace¹. The size of the hybridization matrix is changed accordingly. In our measurement routine for the two-particle Green's function the result from Eq.(4.60) is accumulated for all entries of the inverse hybridization matrix. Each of these single results will be referred to as estimator and we call the set of all these evaluations for a given configuration a measurement.² Thus the number of estimators in each bin per measurement depends on the expansion order as well as on the number of bins. For increasing β the size of the hybridization matrix increases and approaching low temperatures becomes numerically expensive. Opposed to the Hirsch-Fye algorithm, in the hybridization algorithm the matrix size is getting smaller for increasing U (see [26, 27]). In turn, sampling the partition function becomes more efficient in the strong coupling regime. In Figure 5.4 we show the scaling of the overall runtime with β and U for the computation of generalized susceptibilities in the DMFT limit. The corresponding results in τ - and ω -space are shown in Figure 5.5. In all these simulations 10 DMFT-iterations were performed. The simulations for various values of U were done for $\beta = 150$ and we used 10^4 measurements in the first 9 DMFT-iterations at the single-particle level. The two-particle Green's function was evaluated only in the 10th DMFT-iteration using 10^5 measurements. In the simulations for various β were 10^6 (10^7) measurements performed on the single-(two-)particle level. In the simulation for $\beta = 150$ there were 10^4 (10^5) measurements done and the resulting (very

¹As local trace we refer here to the factor $\text{Tr}_c[\dots]$ in Eq.(4.19) which contains the impurity operators.

²The number of measurements can be passed as an external parameter to the algorithm, where the number of estimators results rather indirectly from the expansion order. Both, however, contribute to the statistics and thus to the quality of the result.

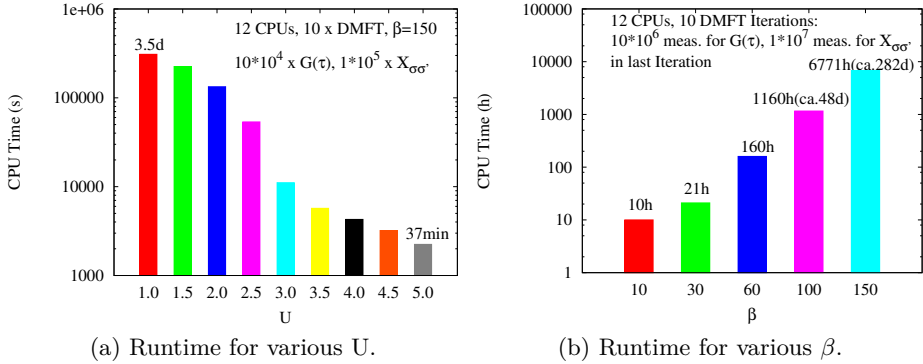


Figure 5.4: Scaling of computation time: DMFT-simulation of the half-filled single-site Hubbard model on the Bethe lattice for different U and β .

long) runtime for 10^6 measurements is only an extrapolation. In testing our measurement routine we made the following observations:

- Since the two-particle Green's function comes with three τ -indices the corresponding statistical effort scales with the third power of the number of bins as opposed to the single-particle case where this scaling is only linear.
- Increasing the number of bins makes the binning error smaller, but the statistical effort and the memory requirement for the computation grow drastically.
- In the strong-coupling regime, the absolute values of the two-particle Green's function become relatively small compared to the weak-coupling regime. In turn a fine discretization, i.e. a fine binning, is necessary to resolve any details of the Green's function.
- Due to the increasing expansion order for high values of β the evaluation time for the two-particle Green's function increases rapidly. The amplitudes are getting smaller but for high expansion orders the number of estimators per bin and measurement increases which, in turn, results in better statistics.

The points above make clear that the preferable scaling for sampling the partition function in the strong coupling regime is not directly transferred to the measurement of the two-particle Green's function. In our simulations

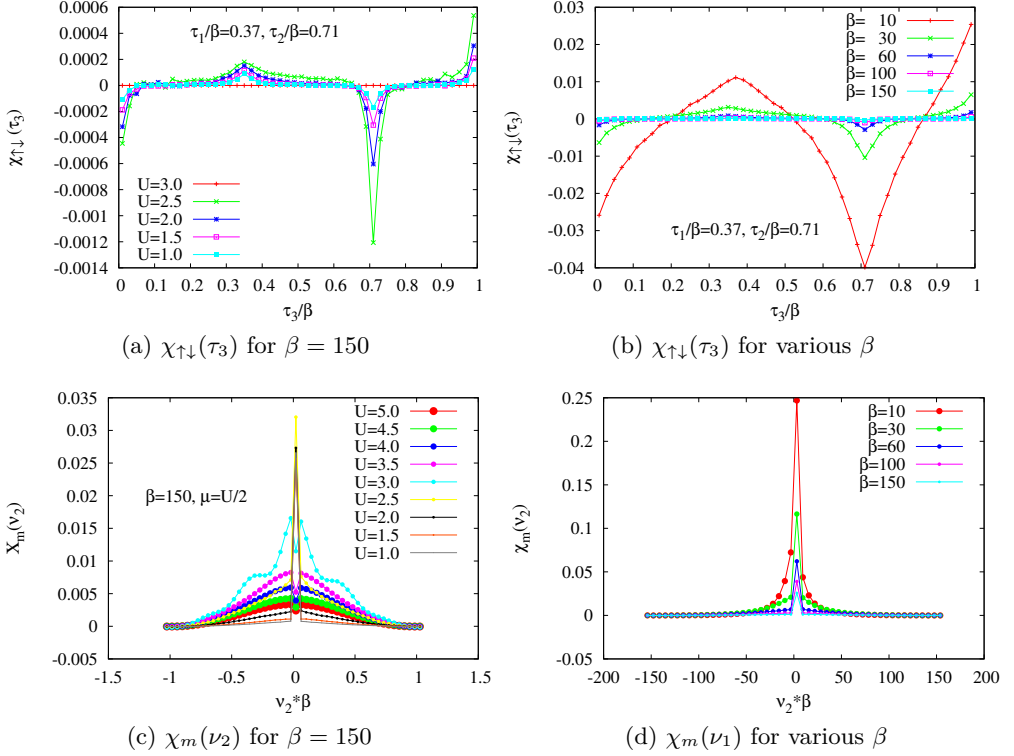


Figure 5.5: Generalized susceptibilities χ in the DMFT-limit at different values of β and U .

we were, due to a lack of computer memory and due to statistical reasons practically restricted to a maximum of 100 bins (for each τ -index).

5.4 First Application: Local Spin Susceptibility

As a first application of our measurement routine, we calculate the behavior of the local spin susceptibility:

$$\chi_{loc}(\omega) := \sum_{\nu\nu'} \chi_m^{\nu\nu'\omega}, \quad (5.5)$$

in the vicinity of the Mott-Hubbard metal-insulator transition (MIT). This phase transition is driven by electron-electron interaction. The correlation induced insulating phase is referred to as Mott insulator. Our main concern here is to test the applicability of our routine to the calculation of χ_{loc} . A detailed discussion about the local spin susceptibility near the MIT at finite

temperature is given in [14, 28]. Zero-temperature results obtained from a projective quantum Monte Carlo algorithm can be found in [29]. We performed calculations for the half-filled Hubbard model with a semicircular density of states (Bethe lattice). The half bandwidth is set to unity. We approach the MIT from the metallic side, i.e. from low values of U initializing the DMFT self-consistency routine with a purely metallic solution ($\Sigma = 0$). At zero temperature (or equiv. $\beta \rightarrow \infty$) and for increasing U the local susceptibility is expected to diverge (see [29]) at the MIT.

In Figure 5.6 we show $\chi_{loc}(0)$ over U for various values of β . In the metallic regime we observe the expected increase of $\chi_{loc}(0)$. With increas-

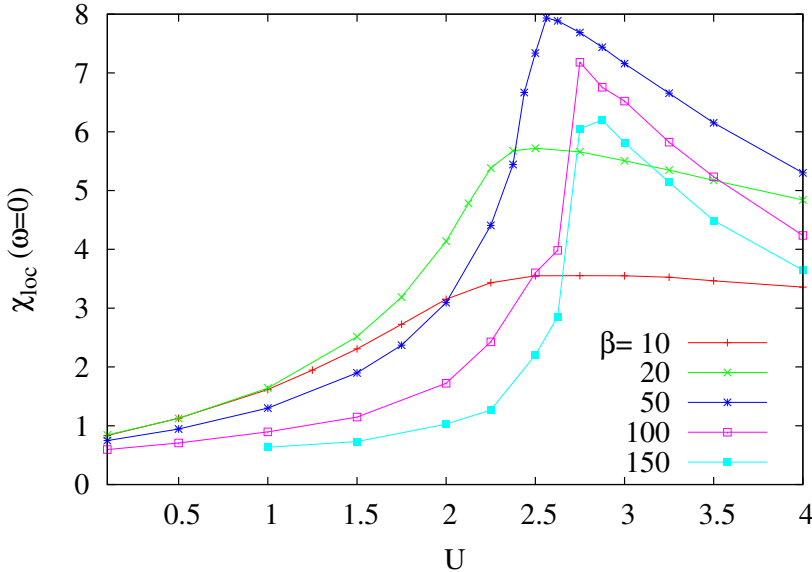


Figure 5.6: Local spin susceptibility for various values of β in the vicinity of the Mott-transition. The simulations are done with 50 bins. We obtain the expected increase of χ_{loc} in the metallic phase, however, we get an unexpected decrease in the insulating phase.

ing β the maximum of χ_{loc} is shifted towards higher values of U . This is consistent with the broadening of the coexistence region in the DMFT solution. Our method, however, fails to predict the constant behavior of $\chi_{loc}(0)$ in the insulating phase. Instead the susceptibility falls off in the insulating regime which is in clear conflict with the results in [14, 28, 29]. We suspect that this incorrect behavior is caused by the systematic error that we introduce in the measurement of the two-particle Green's function at the discontinuities, i.e. the binning error discussed in Chapter 5.1. This suspicion is confirmed by Figure 5.7, where the influence of N_{bin} on χ_m

(left panel) and χ_{loc} (right panel) is shown. From the right panel it can

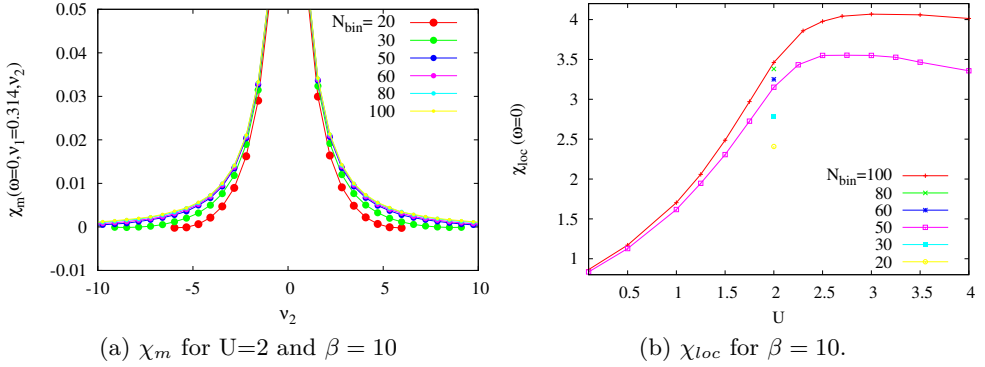


Figure 5.7: Influence of N_{bin} on χ_m and χ_{loc} : (a) for small N_{bin} the systematic offset is clearly noticeable, additionally we miss due to the resulting small N_f non-negligible contributions in the frequency summation; (b) the comparison between χ_{loc} from $N_{bin} = 50$ and $N_{bin} = 100$ suggests that we actually must use at least $N_{bin} > 100$ to get the expected behavior in the insulating phase.

be seen that the unexpected downward trend of χ_{loc} for large values of U is tamed by increasing N_{bin} . Furthermore in our simulations the sum in Eq.(5.5) is done over a finite number N_f of fermionic frequencies ν, ν' . We use a Fourier transformation where N_f is fixed to be equal two times the number of bins N_{bin} . Hence, for $N_{bin} = 50$, the summation in Eq.(5.5) goes over $N_f = 100$ frequencies in each ν and ν' . For small N_f we might miss substantial contributions in this "incomplete" summation (see left panel of Figure 5.7). An accurate evaluation would require some kind of extrapolation prescription in which this frequency cut-off is sent to infinity. Finally we inquire the influence of the statistic on our results. In the parameter regime of low temperature and strong interaction the amplitudes of the two-particle Green's function are approximately a factor 10^{-3} smaller than in the metallic phase (see Figure 5.8). Thus resolving relevant features of the two-particle Green's function requires a fine discretization which, in turn, makes it numerically expensive to reach sufficient statistic to obtain a smooth χ_m .

In the left panel of Figure 5.9 we show the spin susceptibility resulting from different initializations (seeds) of the random-number generator. The right panel shows the average of these results and the corresponding, rather large, error-bars. One might suspect that these results do not form a good basis for the calculation of χ_{loc} . But since we sum up all the values of

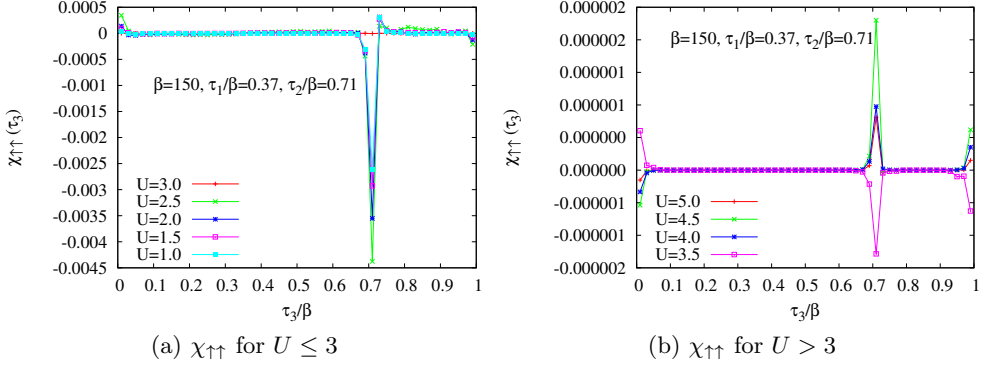


Figure 5.8: $\chi_{\uparrow\uparrow}$ for $\beta = 150$ and various values of U : the amplitudes for $U \geq 3$ are about three orders smaller than for $U < 3$; furthermore between $U = 3.5$ and $U = 4$ a change in the sign of χ can be observed.

the susceptibility for ν_1 and ν_2 the statistical errors are canceling to some extent and we observe that the bad statistic, reflected in the huge error-bars, has practically no influence on the final result for the local susceptibility. We also confirmed this issue at $\beta = 20$ and $U = 3.5$ where we compared calculations which were done with 10^5 and 10^6 measurements and found agreement in the corresponding χ_{loc} up to the third decimal place.

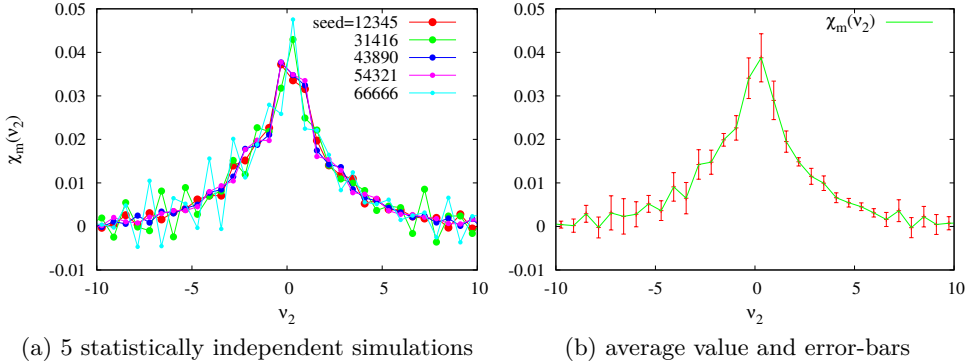


Figure 5.9: Spin susceptibility χ_m at $\beta = 10$ and $U = 5$: (a) results from different initializations (seeds) of the random number generator, in each of these independent simulations 10^7 measurements were performed; (b) average values and the corresponding standard deviation.

Chapter 6

Conclusion and Prospect

We have implemented and tested a measurement routine for the two-particle Green's function in a continuous-time hybridization expansion algorithm. This routine is based on the identification of partition function configurations with two hybridization lines removed as configurations for the two-particle Green's function. Within this approach it is, in contrast to the segment formulation, possible to account for correlation functions which are not diagonal in their band indices. For testing purposes we compared two-particle quantities like the spin susceptibility in the DMFT limit of the single-band Hubbard model from our new routine to those from the Hirsch-Fye and Exact-Diagonalization method. In τ -space representation the only discrepancies in these comparisons appear at those points where two τ -indices of the two-particle Green's function are equal and the disconnected part is discontinuous. The measurement at these discontinuities turned out to be problematic and we did not completely solve this issue. Their importance was not clear at an early stage of this work, so we decided to implement an approximative method to treat these special points of the two-particle Green's function.

In order to benchmark the performance of our code we carried out calculations of two-particle correlation functions at various values of the interaction strength and temperature. It is known that, opposed to the Hirsch-Fye method, in the hybridization algorithm sampling the partition function becomes more efficient with increasing U , i.e. in the strong coupling regime. However, we observe that this favorable scaling with U does not directly transfer to the measurement of the two-particle Green's function. In the hybridization algorithm the averaged expansion order of partition function configurations goes down with increasing U . Therefore less hybridization lines are present in the local trace and measuring the single-

and two-particle quantities becomes inefficient, i.e. the results suffer from bad statistics. This poor yield of hybridization lines in the local trace must be compensated by increasing the number of measurements (and updates) in the Monte Carlo procedure. For decreasing temperature the averaged expansion order grows and so does the number of hybridization lines in the local trace, thus the number of measurements may be reduced without causing bad statistics.

As a first application we calculated the local spin susceptibility in the vicinity of the Mott-transition of the half-filled single-band Hubbard model. In the metallic regime we obtain the expected increase of the susceptibility when approaching the transition point. For the Mott insulator, i.e. at strong interaction, our local susceptibility is in clear conflict with the results found in the literature. Instead of a constant behavior our χ_{loc} decreases with growing U . If we choose a finer τ -grid, i.e. more bins, this discrepancy is getting smaller and the problem most likely originates in our simplified treatment of the discontinuities of the two-particle Green's function. Due to the three τ -indices of the two-particle Green's function the required number of measurements and the numerical effort in doing the Fourier transformation grow drastically with the number of bins, so we were practically restricted to simulations with 100 bins (τ -points). For the case of the local spin susceptibility this already results in an overall simulation time of several days. Owing to the shorter simulation time the majority of our simulations were done with 50 bins which can be performed within a single day. However, it turned out that for 50 bins our method is not accurate enough to predict the expected behavior of the local spin susceptibility in the insulating regime.

Finally we suggest possible further applications and improvements of our routine. The starting point in any extension of the current work must certainly be a more accurate treatment of the discontinuities. After this is done we expect the bad influence of the discretization on our results to be significantly reduced and we might even get on a coarse τ -grid satisfying results for the local susceptibility. Our code features multi-band functionalities providing local Hamiltonians of Slater-Kanamori and Coulomb type. This allows us to run multi-band simulations including non-density-density interactions. A potential future application of our measurement routine would be the investigation of two-particle quantities from multi-band models with these interactions. With the existing code it is in principle possible to perform such calculations. In the current setup we are however restricted to a maximum parallel usage of 12 CPU's on a single node of the computer cluster we utilize. This makes especially the Fourier transformation for

many τ -points very costly in terms of time. In order to make the resulting simulation times reasonable particularly with regard to time-consuming multi-band calculations it would be necessary to improve the parallelization of the code such that several nodes of the computer cluster can be used in parallel.

Bibliography

- [1] M. Born, and R. Oppenheimer, Zur Quantentheorie der Molekeln, *Annalen der Physik*, **389**, 457 (1927).
- [2] P. Hohenberg, and W. Kohn, Inhomogeneous Electron Gas, *Phys. Rev. B* **136**, 864 (1964).
- [3] W. Kohn, and L. J. Sham, Self-Consistent Equations Including Exchange and Correlation Effects, *Phys. Rev. A* **140**, 1133 (1965).
- [4] J. Hubbard, Electron Correlations in Narrow Energy Bands, *Proc. R. Soc. (London) A* **276**, 238 (1963).
- [5] M. C. Gutzwiller, Effect of Correlation on the Ferromagnetism of Transition Metals, *Phys. Rev. Lett.* **10** 159 (1963).
- [6] J. Kanamori, Electron Correlation and Ferromagnetism of Transition Metals, *Progr. Theor. Phys.* **30**, 275 (1963).
- [7] P. W. Anderson, Localized Magnetic States in Metals, *Phys. Rev.* **124**, 41 (1961).
- [8] J. C. Slater, and W. Shockley, Optical Absorption by the Alkali Halides, *Phys. Rev.* **49**, 537 (1936).
- [9] J. Kanamori, Electron Correlation and Ferro magnetism of Transition Metals, *Prog. Theor. Phys.* **30**, 3 (1963).
- [10] G. Rohringer, A. Valli, and A. Toschi, Local Electronic Correlation at the Two-Particle Level, *Phys. Rev. B* **86**, 125114 (2012).
- [11] W. Metzner, and D. Vollhardt, Correlated Lattice Fermions in $d = \infty$ Dimensions, *Phys. Rev. Lett.* **62**, 324 (1989).
- [12] E. Müller-Hartmann, Correlated fermions on a lattice in high dimensions, *Z. Phys. B* **74**, 507 (1988).

- [13] D. Vollhardt, Krzysztof Byczuk, and Marcus Kollar, Dynamical Mean-Field Theory, arXiv:1109.4833v1 (2011).
- [14] A. Georges and G. Kotliar, Hubbard model in infinite dimensions, *Phys. Rev. B* **45**, 6479 (1992).
- [15] A. Georges, G. Kotliar, W. Krauth, and M. J. Rozenberg, Dynamical mean-field theory of strongly correlated fermion systems and the limit of infinite dimensions, *Rev. Mod. Phys.*, **68**, 13 (1996).
- [16] J. E. Hirsch and R. M. Fye, Monte Carlo Method for Magnetic Impurities in Metals, *Phys. Rev. Lett.*, **56**, 2521 (1986).
- [17] A.N. Rubtsov, and A.I. Lichtenstein, Continuous time quantum Monte Carlo method for fermions: beyond auxiliary field framework, *JETP Lett.* **80**, 67 (2004).
- [18] K.Mikelsons, A. Macridin, and M. Jarrell, The relationship between Hirsch-Fye and weak coupling diagrammatic Quantum Monte Carlo methods, *Phys. Rev. E* **79**, 057701 (2009).
- [19] J. Otsuki, H. Kusunose, P. Werner, and Y. Kuramoto, Continuous-Time Quantum Monte Carlo Method for the Coqblin-Schrieffer Model, *J. Phys. Soc. Jpn.* **76**, 114707 (2007).
- [20] P. Werner, A. Comanac, L. Medici, M. Troyer, and A. Millis, A continuous-time solver for quantum impurity models, *Phys. Rev. Lett.* **97**, 076405 (2006).
- [21] P. Werner, and A. Millis, Hybridization expansion impurity solver: General formulation and application to Kondo lattice and two-orbital models, *Phys. Rev. Lett. B* **74**, 155107 (2006).
- [22] E. Gull, and A. Millis, Continuous-time Monte Carlo methods for quantum impurity models, *Rev. Mod. Phys.*, **83**, 349 (2011).
- [23] E. Gull, Continuous-Time Quantum Monte Carlo Algorithms for Fermions, PhD. Thesis, ETH Zürich (2008).
- [24] K. Haule, Quantum Monte Carlo impurity solver for cluster dynamical mean-field theory and electronic structure calculations with adjustable cluster base, *Phys. Rev B* **75**, 155113 (2007).
- [25] A. M. Läuchli, and P. Werner, Krylov-implementation of the hybridization expansion impurity solver and application to 5-orbital models, *Phys. Rev B* **80**, 235117 (2009).

- [26] E. Gull, P. Werner, A. Millis, and M. Troyer, Performance analysis of continuous-time solvers for quantum impurity models, *Phys. Rev. B* **76**, 235123 (2008).
- [27] H. Hafermann, P. Werner, and E. Gull, Efficient implementation of the continuous-time hybridization expansion quantum impurity solver, *Computer Physics Communications* **184**, 1280 (2013).
- [28] M. J. Rozenberg, G. Kotliar, and X.Y. Zhang, Mott-Hubbard transition in infinite dimensions. II, *Phys. Rev. B* **49**, 10181 (1993).
- [29] M. Feldbacher, K. Held, and F.F. Assaad, Projective Quantum Monte Carlo Method for the Anderson Impurity Model and its Application to Dynamical Mean Field Theory, *Phys. Rev. Lett.* **93**, 136405 (2004).
- [30] E. U. Condon, and H. Odabasi, *Atomic Structure*, Cambridge University Press (1980).
- [31] J. D. Jackson, *Classical Electrodynamics*, 3rd edition, John Wiley & Sons (1999).
- [32] C. J. Ballhausen, *Introduction to Ligand Field Theory*, McGraw-Hill (1962).
- [33] N. Zettili, *Quantum Mechanics: Concepts and Applications*, 2nd edition, John-Wiley (2009).
- [34] M.E. Peskin, D.V. Schroeder, *An Introduction to Quantum Field Theory*, Westview (1995).

Appendix A

The Local Hamiltonian for Spherical Symmetric Coulomb Interaction

The purpose of this appendix is to give a detailed derivation of the local Hamiltonian for the case of spherical symmetric Coulomb interaction. The idea is to use the matrix elements of the Coulomb interaction with central field eigenfunctions as the U in the local Hamiltonian. In the calculation of these matrix elements it turns out that the corresponding angular dependent part can be expressed analytically where the radial part can not. The angular part involves integrals over the product of three spherical harmonics. In Appendix A.2 we introduce the so called Gaunt coefficients which give, when expressed in terms of Wigner 3-j symbols (see Appendix A.1), a compact formula to calculate the integral over three spherical harmonics. In Appendix A.3 we finally obtain the desired expression for the local Hamiltonian.

A.1 The Wigner 3-j Symbol

The Wigner 3-j symbol is an algebraic function defined by the following expression [30], also referred to as Racah formula:

$$\begin{aligned}
 \begin{pmatrix} j_1 & j_2 & j_3 \\ m_1 & m_2 & m_3 \end{pmatrix} &\equiv \delta_{m_1+m_2+m_3,0} (-1)^{(j_1-j_2-m_3)} \left[\frac{1}{(j_1+j_2+j_3+1)!} \right]^{1/2} \\
 &\times [(j_1+j_2-j_3)!(j_1-j_2+j_3)!(-j_1+j_2+j_3)!]^{1/2} \\
 &\times [(j_1-m_1)!(j_1+m_1)!(j_2-m_2)!(j_2+m_2)!(j_3-m_3)!(j_3+m_3)!]^{1/2} \\
 &\times \sum_k \frac{(-1)^k}{k!(j_1+j_2-j_3-k)!(j_1-m_1-k)!} \\
 &\times \frac{1}{(j_2+m_2-k)!(j_3-j_2+m_1+k)!(j_3-j_1-m_2+k)!}.
 \end{aligned} \tag{A.1}$$

This function is defined to be non-zero only for values of j_i and m_i such that the arguments of all factorials are non-negative integers. From the first line of (A.1) follows:

$$(j_1 - j_2 - m_3) \in \mathbb{Z} \tag{A.2}$$

and

$$(j_1 + j_2 + j_3) \in \mathbb{N} \tag{A.3}$$

in order that the 3-j symbol is real valued. From the second line follow the conditions:

$$\begin{aligned}
 j_1 + j_2 &\geq j_3, \\
 j_2 + j_3 &\geq j_1, \\
 j_3 + j_1 &\geq j_2.
 \end{aligned} \tag{A.4}$$

From the third line can be seen, that j_i and m_i must both be either integral or half-integral, with $j_i \geq |m_i| \geq 0$. The summation in (A.1) is finite, being over those integral values of k that satisfy

$$\max(0, j_2 - j_3 - m_1, j_1 - j_3 + m_2) \leq k \leq \min(j_1 + j_2 - j_3, j_1 - m_1, j_2 + m_2). \tag{A.5}$$

An important symmetry property of the 3-j symbol follows directly from the definition:

$$\begin{pmatrix} j_1 & j_2 & j_3 \\ -m_1 & -m_2 & -m_3 \end{pmatrix} = (-1)^{j_1+j_2+j_3} \begin{pmatrix} j_1 & j_2 & j_3 \\ m_1 & m_2 & m_3 \end{pmatrix}, \tag{A.6}$$

which, in the special case of $m_1 = m_2 = m_3 = 0$, results in the condition that $(j_1 + j_2 + j_3)$ must be even.

A.2 Gaunt Coefficients

The spherical harmonics $Y_{lm}(\theta, \phi)$ form a complete set for functions of the spherical coordinates θ and ϕ . Since the product of two spherical harmonics is a function of θ and ϕ it can be expanded in spherical harmonics. This gives the Gaunt series:

$$Y_{l_a m_a}(\theta, \phi) Y_{l_c m_c}(\theta, \phi) = \sum_{l=0}^{\infty} \sum_{m=-l}^l Y_{lm}(\theta, \phi) g_{lm}(l_a, m_a; l_c, m_c), \quad (\text{A.7})$$

with the Gaunt coefficients:

$$g_{lm}(l_a, m_a; l_c, m_c) = \int_0^\pi \int_0^{2\pi} d\theta d\phi \sin \theta Y_{lm}^*(\theta, \phi) Y_{l_a m_a}(\theta, \phi) Y_{l_c m_c}(\theta, \phi). \quad (\text{A.8})$$

Using the Wigner 3-j symbols (A.1) allows to express the Gaunt coefficients as follows:

$$g_{lm}(l_a, m_a; l_c, m_c) = (-1)^m \sqrt{\frac{[l][l_a][l_c]}{4\pi}} \begin{pmatrix} l & l_a & l_c \\ 0 & 0 & 0 \end{pmatrix} \begin{pmatrix} l & l_a & l_c \\ -m & m_a & m_c \end{pmatrix}, \quad (\text{A.9})$$

where $[l] = (2l + 1)$.

The relations (A.8) and (A.9) together with (A.1) provide an elegant way to calculate the integral over the product of three spherical harmonics.

A.3 The Matrix Elements of Coulomb Interaction

A system of N interacting identical electrons may be approximated by a set of independent one-electron wave functions $\{\psi(a; \mathbf{x}_1), \psi(b; \mathbf{x}_2), \dots, \psi(n; \mathbf{x}_n)\}$ labelled by an individual set of quantum numbers $\{a, b, \dots, n\}$. For the case of Coulomb interaction the matrix elements of the local interaction Hamiltonian H_U can be written as follows [30]:

$$\begin{aligned} \langle a, b | H_U | c, d \rangle &\equiv \left\langle a, b \left| \frac{1}{|\mathbf{x}_1 - \mathbf{x}_2|} \right| c, d \right\rangle \\ &= \int \int d\mathbf{x}_1 d\mathbf{x}_2 \psi^\dagger(a; \mathbf{x}_1) \psi^\dagger(b; \mathbf{x}_2) \frac{1}{|\mathbf{x}_1 - \mathbf{x}_2|} \psi(c; \mathbf{x}_1) \psi(d; \mathbf{x}_2), \end{aligned} \quad (\text{A.10})$$

where a stands for $\{n_a, l_a, m_a, m_{sa}\}$, also referred to as principal quantum number, the quantum numbers of orbital angular momentum and the z -projection of angular momentum and spin, respectively. The corresponding

wave function reads:

$$\psi(a; \mathbf{x}_1) = R_{n_a l_a}(r_1) Y_{l_a m_a}(\theta_1, \phi_1) \chi_{m_{s_a}}. \quad (\text{A.11})$$

The spin operators \mathbf{S}_1 and \mathbf{S}_2 commute with $\frac{1}{|\mathbf{x}_1 - \mathbf{x}_2|}$. Thus the product of the spinor parts χ_{m_s} in (A.10) results in a pair of Kronecker deltas $\delta_{m_{s_a}, m_{s_c}} \delta_{m_{s_b}, m_{s_d}}$ and the Coulomb Hamiltonian matrix is therefore separately diagonal in the spin indices. That's why in the Coulomb model interacting electrons do not change their spin.

Expanding $\frac{1}{|\mathbf{x}_1 - \mathbf{x}_2|}$ in spherical harmonics $Y_{lm}(\theta, \phi)$ gives [31]:

$$\frac{1}{|\mathbf{x}_1 - \mathbf{x}_2|} = \sum_{l=0}^{\infty} \sum_{m=-l}^l \frac{4\pi}{[l]} \frac{r_{<}^l}{r_{>}^{l+1}} Y_{lm}(\theta_1, \phi_1) Y_{lm}^*(\theta_2, \phi_2), \quad (\text{A.12})$$

where $[l]$ is an abbreviation for $(2l+1)$ and $r_{<}$ ($r_{>}$) is the smaller (greater) value of $|\mathbf{x}_1|$ and $|\mathbf{x}_2|$. Expressing the spherical harmonics in terms of associated Legendre functions $P_{lm}(\cos \theta)$ yields:

$$Y_{lm}(\theta, \phi) = \sqrt{\frac{[l]}{4\pi} \frac{(l-m)!}{(l+m)!}} P_{lm}(\cos \theta) e^{im\phi}. \quad (\text{A.13})$$

Collecting all exponentials in (A.10) and integrating over the azimuthal angles ϕ_i results in the factor:

$$\sum_{m=-l}^l \int_0^{2\pi} d\phi_1 e^{i(m-m_a+m_c)\phi_1} \int_0^{2\pi} d\phi_2 e^{i(m_d-m-m_b)\phi_2}, \quad (\text{A.14})$$

which is only different from zero when $(m - m_a + m_c) = 0$ and $(m_d - m - m_b) = 0$. The factor (A.14) is thus equivalent to the condition [32]:

$$m_a + m_b = m_c + m_d \quad (\text{A.15})$$

which gives another Kronecker delta $\delta_{m_a+m_b, m_c+m_d}$ and removes the sum over m . The Hamiltonian is therefore diagonal in $L_{z_1} + L_{z_2}$ but not separately in L_{z_1} and L_{z_2} , expressing the physical fact that interacting electrons may interchange orbital angular momentum.

The matrix elements (A.10) can now be written as:

$$\langle a, b | H_U | c, d \rangle = \delta_{m_{s_a}, m_{s_c}} \delta_{m_{s_b}, m_{s_d}} \delta_{m_a+m_b, m_c+m_d} \sum_{l=0}^{\infty} g_{lm}(a; c) g_{lm}(b; d) R_l(a, b; c, d), \quad (\text{A.16})$$

where the entire¹ angular dependence is now contained in the Gaunt coefficients $g_{lm}(a; c)$ and $g_{lm}(b; d)$. The special cases $\langle a, b | H_U | a, b \rangle$ and $\langle a, b | H_U | b, a \rangle$ are also referred to as direct and exchange contribution, respectively. The Gaunt coefficients may be used to calculate integrals over three spherical harmonics (see previous section) as required in (A.10). They are related to the Wigner 3-j symbol (A.1) as follows:

$$g_{lm}(a; c) = (-1)^{m_a} \sqrt{\frac{[l_a][l_c][l]}{4\pi}} \begin{pmatrix} l_a & l_c & l \\ 0 & 0 & 0 \end{pmatrix} \begin{pmatrix} l_a & l_c & l \\ -m_a & m_c & m \end{pmatrix}, \quad (\text{A.17})$$

where $m = m_a - m_c$. A definition and some important properties of the 3-j symbol are given in the first section of this appendix. The remaining radial integral $R_l(a, b; c, d)$ is also referred to as Slater integral and reads:

$$R_l(a, b; c, d) = \int_0^\infty \int_0^\infty dr_1 dr_2 r_1^2 r_2^2 \frac{r_1^l}{r_1^{l+1}} R_{n_a l_a}(r_1) R_{n_b l_b}(r_2) R_{n_c l_c}(r_1) R_{n_d l_d}(r_2). \quad (\text{A.18})$$

As a direct consequence of (A.4), the summation over l in (A.16) is finite and reduces to integral values meeting the condition $l \leq \min(l_a + l_c, l_b + l_d)$. According to $l_a + l_c$ is even or odd, l must only take even or odd values. This can be seen from the symmetry property (A.6) of the 3-j symbol for the special case of $\begin{pmatrix} l_a & l_c & l \\ 0 & 0 & 0 \end{pmatrix}$. When only scatter events in one orbital l' are taken into account, l must take even integral values such that $l \leq 2l'$. For example, in the case of d-shell ($l' = 2$) interaction the summation only goes over the values $l = 0, 2, 4$.

The Coulomb Hamiltonian H_U may be written in terms of creation (annihilation) operators and a scattering amplitude $U_{abcd} \equiv \langle a, b | H_U | c, d \rangle$:

$$H_{loc} = \sum_{abcd} U_{abcd} c_a^\dagger c_b^\dagger c_c c_d. \quad (\text{A.19})$$

Restricting (A.19) to scattering processes in a single orbital l and restoring the notation from (2.10) yields the required expression for the impurity model:

$$H_{loc} = \sum_{mnpq\sigma\sigma'} \delta_{m+n, p+q} (-1)^{m+p} [l]^2 c_{m\sigma}^\dagger c_{n\sigma'}^\dagger c_{p\sigma} c_{q\sigma'} \times \sum_{k=0}^{2l} \begin{pmatrix} l & l & k \\ 0 & 0 & 0 \end{pmatrix}^2 \begin{pmatrix} l & l & k \\ -m & p & m-p \end{pmatrix} \begin{pmatrix} l & l & k \\ -n & q & n-q \end{pmatrix} R_k, \quad (\text{A.20})$$

¹The additional delta function $\delta_{m_a+m_b, m_c+m_d}$ in (A.16) is actually redundant, since condition (A.15) is already contained in the Gaunt coefficients.

where $\delta_{m_{sa},m_{sc}}\delta_{m_{sb},m_{sd}}$ is consumed in the spin indices of the creation and annihilation operators. The factor $\frac{4\pi}{[l]}$ from the series expansion (A.12) cancels with factors from (A.17). The Kronecker delta $\delta_{m+n,p+q}$ is actually redundant since it is already contained in the 3-j symbols.

Appendix B

Derivation of Bare Green's Functions using the Equation of Motion Method

In this appendix we derive the solutions for the bare single-particle Green's function using the equation of motion method. We use these results in the DMFT section.

B.1 Bare Green's Function of the Hubbard Model

In the non-interacting limit ($U = 0$) the single-particle Green's function can be expressed analytically. In order to do that, we first define the lattice Fourier transformation which takes the operators to momentum space:

$$c_{k_n\sigma} = \frac{1}{\sqrt{N}} \sum_{m=1}^N e^{ik_n r_m} c_{m\sigma}, \quad (\text{B.1})$$

and the inverse transformation:

$$c_{m\sigma} = \frac{1}{\sqrt{N}} \sum_{n=1}^N e^{-ik_n r_m} c_{k_n\sigma}. \quad (\text{B.2})$$

The above discrete Fourier transformation is valid on a lattice with N sites defined by the lattice vectors r_i and periodic boundary conditions¹, such that the momenta take the discrete values $k_n = \frac{2\pi n}{N}$. In the following we

¹Formally, periodic boundary conditions, are expressed by the identification $(N+i) \sim i$.

will use the short hand notation and simply write k when we actually mean k_n and for the corresponding sum we write \sum_k .

For $U = 0$ in a one dimensional lattice and with the lattice constant set to one, the Hamiltonian takes the simple form:

$$\begin{aligned}
 H &= -t \sum_{\langle m,n \rangle \sigma} c_{m\sigma}^\dagger c_{n\sigma} \\
 &= -t \sum_{m\sigma} [c_{m\sigma}^\dagger c_{m+1,\sigma} + c_{m\sigma}^\dagger c_{m-1,\sigma}] \\
 &= -t \sum_{m\sigma} c_{m\sigma}^\dagger [c_{m+1,\sigma} + c_{m-1,\sigma}].
 \end{aligned} \tag{B.3}$$

Plugging in the operators in momentum representation gives:

$$\begin{aligned}
 H &= -\frac{t}{N} \sum_{m\sigma} \sum_{kq} e^{-ikm} c_{k\sigma}^\dagger (e^{iq(m+1)} + e^{iq(m-1)}) c_{q\sigma} \\
 &= -t \sum_{\sigma} \sum_{kq} \underbrace{\frac{1}{N} \sum_m e^{-i(k-q)m}}_{\delta_{kq}} (e^{iq} + e^{-iq}) c_{k\sigma}^\dagger c_{q\sigma} \\
 &= -\sum_{k\sigma} 2t \cos k c_{k\sigma}^\dagger c_{k\sigma} = \sum_{k\sigma} \epsilon_k c_{k\sigma}^\dagger c_{k\sigma},
 \end{aligned} \tag{B.4}$$

where we have used the orthogonality relation of the Fourier modes e^{ikn} and $\cos k = \frac{e^{ik} + e^{-ik}}{2}$. The resulting Hamiltonian is manifestly momentum conserving, since it is diagonal in momentum space. This is a consequence of the invariance under spatial translations, which we have employed implicitly when we wrote the nearest neighbor site indices as $n = m \pm 1$. It is straightforward to generalize the above result for the dispersion relation ϵ_k to a d -dimensional hyper-cubic lattice:

$$\epsilon_k = -2t \sum_{i=1}^d \cos k_i. \tag{B.5}$$

For arbitrary lattice topology the dispersion relation ϵ_k is given by the lattice Fourier transformation of the corresponding hopping matrix t_{ij} :

$$\epsilon_k = \frac{1}{N} \sum_{lm} e^{i(r_l - r_m)k} t_{lm}, \tag{B.6}$$

with the inverse transformation given by:

$$t_{lm} = \sum_k e^{-i(r_l - r_m)k} \epsilon_k. \tag{B.7}$$

Starting from the definition of the Green's function of the Hubbard Hamiltonian it is possible to derive an analytical expression for the non-interacting case $U = 0$. Therefore we introduce the Heisenberg representation of the momentum space operators:

$$c_k(\tau) = e^{H\tau} c_k e^{-H\tau}, \quad c_k^\dagger(\tau) = e^{H\tau} c_k^\dagger e^{-H\tau}. \quad (\text{B.8})$$

Using the above result in the definition of the Green's function yields:

$$\begin{aligned} G_{mn\sigma}^0(\tau) &= -\langle T_\tau c_{\sigma m}(\tau) c_{\sigma n}^\dagger \rangle \\ &= -\frac{1}{N} \sum_{kq} \delta_{kq} e^{-i(km - qn)} \langle T_\tau c_{k\sigma}(\tau) c_{q\sigma}^\dagger \rangle \\ &= -\frac{1}{N} \sum_k e^{-ik(m-n)} \langle T_\tau c_{k\sigma}(\tau) c_{k\sigma}^\dagger \rangle \end{aligned} \quad (\text{B.9})$$

In the second line we enforce momentum conservation by inserting the Kronecker delta δ_{kq} . In the last line we identify the momentum space representation of the Green's function:

$$G_{k\sigma}^0(\tau) = -\langle T_\tau c_{k\sigma}(\tau) c_{k\sigma}^\dagger \rangle = \frac{1}{N} \sum_{nm} e^{ik(m-n)} G_{mn\sigma}^0(\tau) \quad (\text{B.10})$$

We will also need the following version of the Heisenberg equation of motion:

$$\begin{aligned} \frac{\partial A(\tau)}{\partial \tau} &= \frac{\partial}{\partial \tau} (e^{H\tau} A e^{-H\tau}) \\ &= H e^{H\tau} A e^{-H\tau} - e^{H\tau} A e^{-H\tau} H \\ &= e^{H\tau} H e^{-H\tau} e^{H\tau} A e^{-H\tau} - e^{H\tau} A e^{-H\tau} e^{H\tau} H e^{-H\tau} \\ &= e^{H\tau} [H, A] e^{-H\tau} = [H, A](\tau). \end{aligned} \quad (\text{B.11})$$

Taking the τ -derivative of the Green's function and employing the above result gives:

$$\begin{aligned} \frac{\partial}{\partial \tau} G_{k\sigma}^0(\tau) &= -\langle [H, c_{k\sigma}](\tau) c_{k\sigma}^\dagger \rangle \theta(\tau) - \langle c_{k\sigma}(\tau) c_{k\sigma}^\dagger \rangle \delta(\tau) \\ &\quad + \langle c_{k\sigma}^\dagger [H, c_{k\sigma}](\tau) \rangle \theta(-\tau) - \langle c_{k\sigma}^\dagger c_{k\sigma}(\tau) \rangle \delta(\tau) \\ &= -\langle T_\tau [H, c_{k\sigma}](\tau) c_{k\sigma}^\dagger \rangle - \underbrace{\langle \{c_{k\sigma}(\tau), c_{k\sigma}^\dagger\} \rangle}_{=1} \delta(\tau). \end{aligned} \quad (\text{B.12})$$

For the commutator we get:

$$\begin{aligned}
[H, c_{k\sigma}] &= \sum_{q\sigma'} \epsilon_q [c_{q\sigma'}^\dagger c_{q\sigma'}, c_{k\sigma}] \\
&= \sum_{q\sigma'} \epsilon_q (c_{q\sigma'}^\dagger c_{q\sigma'} c_{k\sigma} - c_{k\sigma} c_{q\sigma'}^\dagger c_{q\sigma'}) \\
&= - \sum_{q\sigma'} \epsilon_q (c_{q\sigma'}^\dagger c_{k\sigma} c_{q\sigma'} + c_{k\sigma} c_{q\sigma'}^\dagger c_{q\sigma'}) \\
&= - \sum_{q\sigma'} \epsilon_q \underbrace{\{c_{q\sigma'}^\dagger, c_{k\sigma}\}}_{\delta_{kq}\delta_{\sigma\sigma'}} c_{q\sigma'} = -\epsilon_k c_{k\sigma}
\end{aligned} \tag{B.13}$$

Using the result for the commutator and writing the Green's function and the delta function in terms of Matsubara frequencies gives for the r.h.s of Eq.(B.12):

$$\begin{aligned}
-\langle T_\tau [H, c_{k\sigma}](\tau) c_{k\sigma}^\dagger \rangle - \delta(\tau) &= \epsilon_k \langle T_\tau c_{k\sigma}(\tau) c_{k\sigma}^\dagger \rangle - \delta(\tau) \\
&= - \sum_n e^{-i\omega_n \tau} (\epsilon_k G_{k\sigma}^0(i\omega_n) + 1),
\end{aligned} \tag{B.14}$$

and for the l.h.s. we find:

$$\sum_n \frac{\partial}{\partial \tau} e^{-i\omega_n \tau} G_{k\sigma}^0(i\omega_n) = - \sum_n i\omega_n e^{-i\omega_n \tau} G_{k\sigma}^0(i\omega_n). \tag{B.15}$$

By comparison of coefficients follows the desired result for the bare Green's function of the Hubbard Hamiltonian:

$$\begin{aligned}
i\omega_n G_{k\sigma}^0(i\omega_n) &= \epsilon_k G_{k\sigma}^0(i\omega_n) + 1 \\
G_{k\sigma}^0(i\omega_n) &= \frac{1}{i\omega_n - \epsilon_k}.
\end{aligned} \tag{B.16}$$

The extension to the multi-orbital case is straight forward:

$$G_{k\alpha}^0(i\omega_n) = \frac{1}{i\omega_n - \epsilon_{k\alpha}}. \tag{B.17}$$

Using the inverse lattice Fourier transform Eq.(B.7) gives:

$$G_{ij\alpha}^0(i\omega_n) = [i\omega_n - t_{ij}]^{-1}. \tag{B.18}$$

By employing Dyson's equation, we get the following expression for the interacting case:

$$G_{k\alpha}(i\omega_n) = \frac{1}{i\omega_n - \epsilon_{k\alpha} - \Sigma_\alpha(k, i\omega_n)}. \tag{B.19}$$

B.2 Bare Green's Function of the Anderson Impurity Hamiltonian

Deriving the bare Green's function \mathcal{G}^0 of the Anderson impurity Hamiltonian is very similar to the procedure above. The essential differences are that we have now two kinds of operators, the impurity operators c_σ and the bath operators $a_{k\sigma}$. In the non-interacting limit the AIM Hamiltonian takes the following form:

$$H = \mu \sum_{\sigma} c_{\sigma}^{\dagger} c_{\sigma} + \sum_{k,\sigma} \epsilon_k a_{k\sigma}^{\dagger} a_{k\sigma} + \sum_{k,\sigma} \left(V_k^{\sigma} a_{k\sigma}^{\dagger} c_{\sigma} + h.c. \right). \quad (\text{B.20})$$

Our aim is to obtain an explicit expression for the bare impurity Green's function:

$$\mathcal{G}_{\sigma}^0(\tau) = -\langle T_{\tau} c_{\sigma}(\tau) c_{\sigma}^{\dagger} \rangle. \quad (\text{B.21})$$

Taking the τ -derivative gives, in complete analogy to above, the following expression:

$$\frac{\partial \mathcal{G}_{\sigma}^0(\tau)}{\partial \tau} = -\langle T_{\tau} [H, c_{\sigma}] (\tau) c_{\sigma}^{\dagger} \rangle - \delta(\tau) \quad (\text{B.22})$$

Next we need to evaluate the commutator:

$$\begin{aligned} [H, c_{\sigma}] &= \sum_{k\sigma'} \epsilon_k [a_{k\sigma'}^{\dagger} a_{k\sigma'}, c_{\sigma}] + \mu \sum_{\sigma'} [c_{\sigma'}^{\dagger} c_{\sigma'}, c_{\sigma}] \\ &\quad + \sum_{k\sigma'} (V_k^{\sigma'} [a_{k\sigma'}^{\dagger} c_{\sigma'}, c_{\sigma}] + V_k^{\sigma'*} [c_{\sigma'}^{\dagger} a_{k\sigma'}, c_{\sigma}]). \end{aligned} \quad (\text{B.23})$$

The first commutator obviously vanishes, and the second one evaluates, in complete analogy to the Hubbard Hamiltonian above, to:

$$\mu \sum_{\sigma'} [c_{\sigma'}^{\dagger} c_{\sigma'}, c_{\sigma}] = -\mu c_{\sigma}. \quad (\text{B.24})$$

The third one vanishes:

$$\begin{aligned} \sum_{k\sigma'} V_k^{\sigma'} [a_{k\sigma'}^{\dagger} c_{\sigma'}, c_{\sigma}] &= \sum_{k\sigma'} V_k^{\sigma'} (a_{k\sigma'}^{\dagger} c_{\sigma'} c_{\sigma} - c_{\sigma} a_{k\sigma'}^{\dagger} c_{\sigma'}) \\ &= \sum_{k\sigma'} V_k^{\sigma'} a_{k\sigma'}^{\dagger} \{c_{\sigma'}, c_{\sigma}\} = 0, \end{aligned} \quad (\text{B.25})$$

and for the last one we find:

$$\begin{aligned} \sum_{k\sigma'} V_k^{\sigma'*} [c_{\sigma'}^{\dagger} a_{k\sigma'}, c_{\sigma}] &= \sum_{k\sigma'} V_k^{\sigma'*} (c_{\sigma'}^{\dagger} a_{k\sigma'} c_{\sigma} - c_{\sigma} c_{\sigma'}^{\dagger} a_{k\sigma'}) \\ &= - \sum_{k\sigma'} V_k^{\sigma'*} (c_{\sigma'}^{\dagger} c_{\sigma} a_{k\sigma'} + c_{\sigma} c_{\sigma'}^{\dagger} a_{k\sigma'}) \\ &= - \sum_{k\sigma'} V_k^{\sigma'*} \underbrace{\{c_{\sigma'}^{\dagger}, c_{\sigma}\}}_{\delta_{\sigma\sigma'}} a_{k\sigma'} = - \sum_k V_k^{\sigma*} a_{k\sigma}. \end{aligned} \quad (\text{B.26})$$

Plugging this in gives:

$$\frac{\partial \mathcal{G}_\sigma^0(\tau)}{\partial \tau} = \mu \underbrace{\langle T_\tau c_\sigma(\tau) c_\sigma^\dagger \rangle}_{=-\mathcal{G}_\sigma^0(\tau)} + \sum_k V_k^{\sigma*} \underbrace{\langle T_\tau a_{k\sigma}(\tau) c_\sigma^\dagger \rangle}_{=-F_{k\sigma}(\tau)} - \delta(\tau) \quad (\text{B.27})$$

The derivative of the mixed operator Green's function $F_{k\sigma}(\tau)$ results in:

$$\frac{\partial F_{k\sigma}(\tau)}{\partial \tau} = -\langle T_\tau [H, a_{k\sigma}](\tau) c_\sigma^\dagger \rangle - \delta(\tau) \underbrace{\langle \{a_{k\sigma}, c_\sigma^\dagger\} \rangle}_{=0}, \quad (\text{B.28})$$

where the commutator evaluates to:

$$[H, a_{k\sigma}] = -\epsilon_k a_{k\sigma} - V_k^\sigma c_\sigma \quad (\text{B.29})$$

Expressing the mixed operator Green's function in terms of Matsubara frequencies and substituting the above expression for the commutator gives:

$$-\sum_n e^{-i\omega_n \tau} (i\omega_n - \epsilon_k) F_{k\sigma}(i\omega_n) = -\sum_n e^{-i\omega_n \tau} V_k^\sigma \mathcal{G}_\sigma^0(i\omega_n) \quad (\text{B.30})$$

This allows to express the mixed operator Green's function as:

$$F_{k\sigma}(i\omega_n) = \frac{V_k^\sigma}{i\omega_n - \epsilon_k} \mathcal{G}_\sigma^0(i\omega_n) \quad (\text{B.31})$$

The series expansion of Eq.(B.22) reads:

$$-\sum_n e^{-i\omega_n \tau} (i\omega_n - \mu) \mathcal{G}_\sigma^0(i\omega_n) = -\sum_n e^{-i\omega_n \tau} \left(\sum_k V_k^{\sigma*} F_{k\sigma}(i\omega_n) + 1 \right) \quad (\text{B.32})$$

Substituting Eq.(B.31) and comparing coefficients gives the explicit expression for the bare Green's function of the AIM:

$$1 = \left(i\omega_n - \mu - \sum_k \frac{|V_k^\sigma|^2}{i\omega_n - \epsilon_k} \right) \mathcal{G}_\sigma^0(i\omega_n) \quad (\text{B.33})$$

$$\mathcal{G}_\sigma^0(i\omega_n) = \left(i\omega_n - \mu - \sum_k \frac{|V_k^\sigma|^2}{i\omega_n - \epsilon_k} \right)^{-1}$$

Extension to the multi orbital case is again straight forward:

$$\mathcal{G}_\alpha^0(i\omega_n) = \left(i\omega_n - \mu - \sum_k \frac{|V_k^\alpha|^2}{i\omega_n - \epsilon_k} \right)^{-1} \quad (\text{B.34})$$

and the Green's function of the interacting system may be expressed as:

$$\mathcal{G}_\alpha(i\omega_n) = \left(i\omega_n - \mu - \sum_k \frac{|V_k^\alpha|^2}{i\omega_n - \epsilon_k} - \Sigma_\alpha(k, i\omega_n) \right)^{-1} \quad (\text{B.35})$$

Appendix C

The Partition Function Expansion

The purpose of this appendix is to demonstrate in detail how we obtain the partition function expansion given in Eq.(4.3).

By splitting the Hamiltonian

$$H = H_a + H_b, \quad (\text{C.1})$$

and introducing an interaction representation in which the imaginary time evolution of operators \mathcal{O} is given by H_a :

$$\mathcal{O}(\tau) = e^{H_a\tau} \mathcal{O} e^{-H_a\tau}. \quad (\text{C.2})$$

the partition function may be written as:

$$Z = \text{Tr} \left[e^{-\beta H} \right] = \text{Tr} \left[e^{-\beta H_a} \underbrace{e^{\beta H_a} e^{-\beta H}}_{U(\beta)} \right] \quad (\text{C.3})$$

We want to express the operator $U(\beta)$ in terms of H_b . First we differentiate it w.r.t. β and keep in mind that H and H_a generally do not commute:

$$\begin{aligned} \frac{dU(\beta)}{d\beta} &= H_a U(\beta) - e^{\beta H_a} H e^{-\beta H} \\ &= H_a U(\beta) - e^{\beta H_a} (H_a + H_b) e^{-\beta H_a} \underbrace{e^{\beta H_a} e^{-\beta H}}_{U(\beta)} \\ &= H_a U(\beta) - H_a U(\beta) - H_b U(\beta) = -H_b U(\beta) \end{aligned} \quad (\text{C.4})$$

Since we know that $U(0) = I$ we can integrate the resulting differential

equation

$$\begin{aligned}
 U(\beta) - U(0) &= - \int_0^\beta d\tau H_b(\tau) U(\tau) \\
 U(\beta) &= I - \int_0^\beta d\tau H_b(\tau) U(\tau).
 \end{aligned}
 \tag{C.5}$$

Iterating this integral equation gives the Dyson series for $U(\beta)$ [33]:

$$\begin{aligned}
 U(\beta) = & I - \int_0^\beta d\tau H_b(\tau) + (-1)^2 \int_0^\beta d\tau_1 H_b(\tau_1) \int_0^{\tau_1} d\tau_2 H_b(\tau_2) \dots \\
 & + (-1)^n \int_0^\beta d\tau_1 H_b(\tau_1) \int_0^{\tau_1} d\tau_2 H_b(\tau_2) \dots \int_0^{\tau_{n-1}} d\tau_n H_b(\tau_n) \dots
 \end{aligned}
 \tag{C.6}$$

It is important to note that the various factors of $H(\tau_i)$ are ordered such that greater values of τ stand on the left. We therefore can use the ordering symbol T_τ to simplify the above expression considerably. A n^{th} order term can be written as

$$\int_0^\beta d\tau_1 \int_0^{\tau_1} d\tau_2 \dots \int_0^{\tau_{n-1}} d\tau_n H_b(\tau_1) \dots H_b(\tau_n) = \frac{1}{n!} \int_0^\beta d\tau_1 \dots \int_0^\beta d\tau_n T_\tau H_b(\tau_1) \dots H_b(\tau_n),
 \tag{C.7}$$

where we used the fact that the integral on the right-hand side counts everything $n!$ times, since the integrand is symmetric about the hyperplane $\tau_1 = \tau_2 = \dots = \tau_n$ [34]. We can now write $U(\beta)$ in a very compact form:

$$U(\beta) = \sum_{n=0}^{\infty} \frac{(-1)^n}{n!} \int_0^\beta d\tau_1 \dots \int_0^\beta d\tau_n T_\tau H_b(\tau_1) \dots H_b(\tau_n) \equiv T_\tau e^{-\int_0^\beta d\tau H_b(\tau)}.
 \tag{C.8}$$

By plugging the above result into Eq.(C.3) gives:

$$\begin{aligned}
 Z &= \text{Tr} \left[e^{-\beta H_a} T_\tau e^{-\int_0^\beta d\tau H_b(\tau)} \right] \\
 &= \text{Tr} \left[e^{-\beta H_a} \sum_{k=0}^{\infty} \frac{(-1)^k}{k!} \int_0^\beta d\tau_1 \dots \int_0^\beta d\tau_k T_\tau H_b(\tau_1) \dots H_b(\tau_k) \right].
 \end{aligned}
 \tag{C.9}$$

Using the linear property of the trace allows us to pull the sums in the front of the trace such that we finally obtain the desired expression for the partition function expansion:

$$Z = \sum_{n=0}^{\infty} \int_0^{\beta} d\tau_1 \dots \int_0^{\beta} d\tau_n \frac{(-1)^n}{n!} \text{Tr} \left[T_{\tau} e^{-(\beta-\tau_1)H_a} H_b \dots e^{-(\tau_{n-1}-\tau_k)H_a} H_b e^{-\tau_n H_a} \right] \quad (\text{C.10})$$

Appendix D

The Derivative of a Determinant

As starting point we use the Jacobi formula which gives the first derivative of the determinant of a matrix:

$$\frac{\partial}{\partial A_{ab}} \det A = \det A (A^{-1})_{ba}. \quad (\text{D.1})$$

To get the second derivative we obviously have to apply Jacobi's formula recursively:

$$\begin{aligned} \frac{\partial^2}{\partial A_{ij} \partial A_{kl}} \det A &= \frac{\partial}{\partial A_{kl}} (\det(A) A_{ji}^{-1}) \\ &= \frac{\partial}{\partial A_{kl}} (\det(A)) A_{ji}^{-1} + \det(A) \frac{\partial A_{ji}^{-1}}{\partial A_{kl}}. \end{aligned} \quad (\text{D.2})$$

Now we are faced the problem of taking the derivative of the inverse matrix which we obtain as follows:

$$\begin{aligned} (AA^{-1}) &= I \\ (AA^{-1})' &= I' = 0 \\ (AA^{-1})' &= A' A^{-1} + A (A^{-1})' = 0 \\ (A^{-1})' &= -A^{-1} A' A^{-1}. \end{aligned} \quad (\text{D.3})$$

Inserting this into the equation above gives:

$$\frac{\partial^2}{\partial A_{ij} \partial A_{kl}} \det A = \det A \left[(A^{-1})_{lk} (A^{-1})_{ji} - (A^{-1})_{ad} (A^{-1})_{cb} \right]. \quad (\text{D.4})$$

Appendix E

Hirsch-Fye Method

Prior to continuous-time solvers the discrete time algorithm due to Hirsch and Fye [16] established as the standard method in the simulation of quantum impurity models. The Hirsch-Fye algorithm is based on a discretization of the τ -interval $[0, \beta)$ and the introduction of an auxiliary Ising spin field that allows to decouple the interaction term $H_U = U n_{\uparrow} n_{\downarrow}$ in the impurity model Hamiltonian of Eq.(2.10). As a first step the Hamiltonian of the AIM is rewritten as $H = H_0 + H_I$, where:

$$H_0 = \left(\mu + \frac{U}{2}\right) \sum_{\sigma} n_{\sigma} + \sum_{k, \sigma} \epsilon_k a_{k\sigma}^{\dagger} a_{k\sigma} + \sum_{k, \sigma} (V_k^{\sigma} a_{k\sigma}^{\dagger} c_{\sigma} + \text{h.c.}), \quad (\text{E.1})$$

$$H_I = U[n_{\uparrow} n_{\downarrow} - \frac{1}{2}(n_{\uparrow} + n_{\downarrow})]. \quad (\text{E.2})$$

By applying a so-called Trotter discretization the imaginary time interval $[0, \beta)$ is broken into M slices of equal length $\Delta\tau = \frac{\beta}{M}$. Now the partition function is written as the following product:

$$Z = \text{Tr} e^{-\beta H} = \text{Tr} \prod_{i=1}^M e^{-\Delta\tau(H_0 + H_I)} \approx \text{Tr} \prod_{i=1}^M e^{-\Delta\tau H_0} e^{-\Delta\tau H_I}. \quad (\text{E.3})$$

In the last step we have used the Trotter-Suzuki formula and neglected terms of $O[\Delta\tau^2]$. This results in a systematic error because $e^{-\Delta\tau H_0} e^{-\Delta\tau H_I}$ rather than $e^{-\Delta\tau H}$ is used for the time evolution between the time slices. The central idea is now to introduce an auxiliary spin field on each time slice to decouple the interaction term:

$$e^{-\Delta\tau U(n_{\uparrow} n_{\downarrow} - (n_{\uparrow} + n_{\downarrow})/2)} = \frac{1}{2} \sum_{s_i = \pm 1} e^{\lambda s_i (n_{\uparrow} n_{\downarrow})}, \quad (\text{E.4})$$

with $\cosh\lambda = e^{\frac{1}{2}\Delta\tau U}$. Substituting the above expression into Eq.(E.3) allows, after some manipulation [15], to write the partition function in the following form:

$$Z = \sum_{\{s_j\}} \prod_{\sigma=\pm 1} \det[G_{\sigma}^{\{s_j\}}]^{-1}, \quad (\text{E.5})$$

where the Green's function $G_{\sigma}^{\{s_i\}}$ that corresponds to a particular field configuration $\{s_i\}$ is given by the Dyson equation:

$$G_{\sigma}^{\{s_i\}} = \mathcal{G}_{\sigma}^0 + \mathcal{G}_{\sigma}^0 (\mathbf{I} - e^{\lambda W_{\sigma}^{\{s_i\}}}) G_{\sigma}^{\{s_i\}}, \quad (\text{E.6})$$

with $W_{\sigma}^{\{s_i\}} = \text{diag}(\sigma s_i)$. The sum of Eq.(E.5) is sampled over the 2^M dimensional space of configurations $\mathcal{C} = \{s\}$ with weight $\prod_{\sigma=\pm 1} \det[G_{\sigma}^{\{s_i\}}]^{-1}$.

This method comes, however, with several drawbacks. First of all, the discretization introduces a systematic error. Furthermore the requirement of an equally spaced τ -grid makes the access to low temperatures numerically expensive. Decoupling arbitrary interactions with an auxiliary field is problematic which makes the method practicable for density-density type interactions only. These drawbacks were some of the motivations to look for alternatives leading to continuous-time methods.